AD-A191 425 EFFECTS OF TRANSLATIONAL AND ROTATIONAL NONEQUILIBRIUM ON CW CHEMICAL LAS..(U) AEROSPACE CORP EL SEGUNDO CA AEROPHYSICS LAB H MIRELS 01 MAR 88 TR-0086A(2860)-1 1/1

UNCLASSIFIED SD-TR-88-40 F04701-85-C-0086 F/G 9/3 NL

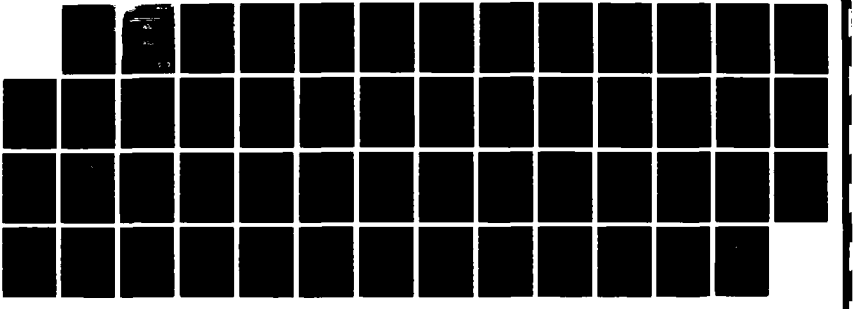

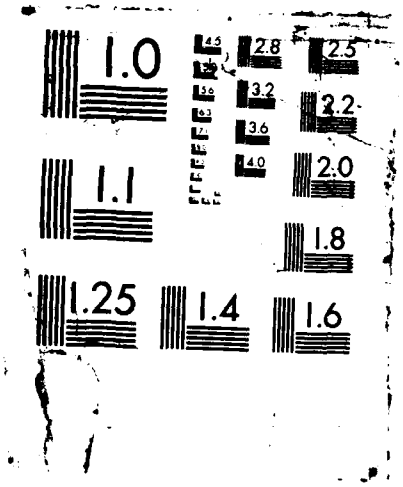
1.0
1.1
1.25
1.4
1.6
1.8
2.0
2.2
2.5
2.8
3.2
3.6
4.0

Translational and Rotational [illegible] on Ew Chemical Laser Performance

B. MIRELS
Aerophysics Laboratory
Laboratory Operations
The Aerospace Corporation
El Segundo, CA 90245

1 March 1988

Prepared for
SPACE DIVISION
AIR FORCE SYSTEMS COMMAND
Los Angeles Air Force Base
P.O. Box 92960, Worldway Postal Center
Los Angeles, CA 90009-2960

This report was submitted by The Aerospace Corporation, El Segundo, CA 90245, under Contract No. F04701-85-C-0086-P00016 with the Space Division, P.O. Box 92960, Worldway Postal Center, Los Angeles, CA 90009-2960. It was reviewed and approved for The Aerospace Corporation by W. P. Thompson, Jr., Director, Aerophysics Laboratory. Lt Scott W. Levinson/CNW was the Air Force project officer.

This report has been reviewed by the Public Affairs Office (PAS) and is releasable to the National Technical Information Service (NTIS). At NTIS, it will be available to the general public, including foreign nationals.

This technical report has been reviewed and is approved for publication. Publication of this report does not constitute Air Force approval of the report's findings or conclusions. It is published only for the exchange and stimulation of ideas.

Scott W. Levinson

SCOTT W. LEVINSON, Lt., USAF
Project Officer
SD/CNW

Raymond M Leong

RAYMOND M. LEONG, Major, USAF
Deputy Director, AFSTC West Coast Office
AFSTC/WCO OL-AB

UNCLASSIFIED
SECURITY CLASSIFICATION OF THIS PAGE

REPORT DOCUMENTATION PAGE

1a. REPORT SECURITY CLASSIFICATION Unclassified	1b. RESTRICTIVE MARKINGS
2a. SECURITY CLASSIFICATION AUTHORITY	3. DISTRIBUTION / AVAILABILITY OF REPORT Approved for public release; distribution unlimited
2b. DECLASSIFICATION / DOWNGRADING SCHEDULE	
4. PERFORMING ORGANIZATION REPORT NUMBER(S) TR-0086A(2060)-1	5. MONITORING ORGANIZATION REPORT NUMBER(S) SD-TR-88-40
6a. NAME OF PERFORMING ORGANIZATION The Aerospace Corporation Laboratory Operations 6b. OFFICE SYMBOL (If applicable)	7a. NAME OF MONITORING ORGANIZATION Space Division
6c. ADDRESS (City, State, and ZIP Code) El Segundo, CA 90245	7b. ADDRESS (City, State, and ZIP Code) Los Angeles Air Force Station Los Angeles, CA 90009-2960
8a. NAME OF FUNDING / SPONSORING ORGANIZATION 8b. OFFICE SYMBOL (If applicable)	9. PROCUREMENT INSTRUMENT IDENTIFICATION NUMBER F04701-85-C-0086-P00016
8c. ADDRESS (City, State, and ZIP Code)	10. SOURCE OF FUNDING NUMBERS PROGRAM ELEMENT NO. / PROJECT NO. / TASK NO. / WORK UNIT ACCESSION NO.

11. TITLE (Include Security Classification)
Effects of Translational and Rotational Nonequilibrium on cw Chemical Laser Performance

12. PERSONAL AUTHOR(S)
Mirels, Harold

13a. TYPE OF REPORT	13b. TIME COVERED FROM ____ TO ____	14. DATE OF REPORT (Year, Month, Day)	15. PAGE COUNT
		1988 March 1	49

16. SUPPLEMENTARY NOTATION

17. COSATI CODES		
FIELD	GROUP	SUB-GROUP

18. SUBJECT TERMS (Continue on reverse if necessary and identify by block number)
Chemical Laser Model,
~~CW~~ Chemical Lasers, (Continuous Wave Chemical Lasers)

19. ABSTRACT (Continue on reverse if necessary and identify by block number)

A previous model used to describe continuous wave (cw) chemical laser performance is generalized to include rotational as well as translational nonequilibrium. The resultant equations are simplified by the realistic assumption that translational and rotational relaxation rates are fast compared with convection, chemical pumping, and collisional deactivation rates. As a consequence, translational and rotational relaxation are in equilibrium with stimulated emission. A further simplification is introduced by the assumption $|R_r/R_t - 1|(\Delta\nu_h/\Delta\nu_d) \ll 1$, where R_r/R_t is the ratio of rotational to translational relaxation rates and $\Delta\nu_h/\Delta\nu_d$ is the ratio of homogeneous to Doppler widths. The resultant system of equations is independent of rotational relaxation. An amplifier solution is presented that predicts saturation effects in accord with experiments. Fabry-Perot oscillator solutions are also presented for a multiline saturated laser and for a partly saturated single-line laser. The present results provide a basis for simplification of numerical codes. It is concluded that a reasonable first estimate for cw chemical laser performance can be obtained by assuming rotational equilibrium and translational nonequilibrium.

20. DISTRIBUTION / AVAILABILITY OF ABSTRACT ☐ UNCLASSIFIED/UNLIMITED ☒ SAME AS RPT ☐ DTIC USERS	21. ABSTRACT SECURITY CLASSIFICATION Unclassified
22a. NAME OF RESPONSIBLE INDIVIDUAL	22b. TELEPHONE (Include Area Code) / 22c. OFFICE SYMBOL

DD FORM 1473, 84 MAR 83 APR edition may be used until exhausted
All other editions are obsolete

SECURITY CLASSIFICATION OF THIS PAGE
UNCLASSIFIED

18. SUBJECT TERMS (Continued)

Inhomogeneous Broadening Effects
Lasers
Multiline Performance
Rotational Nonequilibrium
Translational Nonequilibrium

CONTENTS

I. INTRODUCTION..... 7

II. FORMULATION..... 9

A. Flow Model..... 9

B. Distribution Functions..... 9

C. Laser Equations..... 12

III. EQUILIBRIUM CASES..... 17

IV. NONEQUILIBRIUM CASES..... 19

A. Simplified Equations..... 19

B. Amplifier..... 26

C. Oscillator..... 35

V. DISCUSSION..... 41

VI. CONCLUDING REMARKS..... 43

APPENDIX A: PARTIAL LIST OF SYMBOLS..... 45

APPENDIX B: PARAMETER EVALUATION..... 47

REFERENCES..... 53

FIGURES

1. Continuous Wave Chemical Laser (a) Flow Field and Fabry-Perot Resonator and (b) Flame Sheet Model of Reaction Zone..... 10

2. Variation of Inversion Number Density with Streamwise Distance for Case of Uniformly Illuminated Amplifier with Laminar Mixing..... 27

3. Line Shape for Laser Medium with Single Transition at X_j = 0.0 or 0.4 and a Homogeneous Width $\Delta\nu_h/\Delta\nu_d$ = 0.024; (a) Case X_j = 0.0; (b) Case X_j = 0.4..... 29,30

4. Variation of Gain with Frequency at Streamwise Station ζ = 0.305 in a Uniformly Illuminated Amplifier with a Single Transition at X_j = 0.4; (a) Case $\Delta\nu_h/\Delta\nu_d$ = 0.024; (b) Case $\Delta\nu_h/\Delta\nu_d$ = 0.048..... 31,32

5. Effect of Input Intensity on Line Center ($\nu = \nu_o$) Gain at Fixed Streamwise Station for Uniformly Illuminated Amplifier..... 34

6. Performance of Saturated Multiline Fabry-Perot Oscillator in the Limit $R_r = R_t \gg 1$, $\Delta\nu_h \ll \Delta\lambda_c$, $Y_{J,j} \ll 1$, $G_c \to 0$, and $S = 0(1)$..... 38

7. Performance of Single Line Fabry-Perot Oscillator in Limit $R_r = R_t \gg 1$ and $Y_{j,j} \ll 1$..... 40

TABLES

I. Numerical Values of Parameters for cw HF Laser..... 20-23

II. Maxima for Amplifier with Uniform Incident Radiation and Laminar Diffusion..... 28

III. Homogeneous Width and Gas Kinetic Collision Rate Data for $HF + M_i \rightarrow HF + M_i$..... 48

IV. Vibrational Deactivation Rates for Reaction $HF(v + 1) + M_i \overset{\bar{K}^i_{cd}}{\rightarrow} HF(v) + M_i$..... 50

V. Maximum Value of $\bar{f}_J$ and Corresponding Value of J for fixed θ_R 51

I. INTRODUCTION

Continuous wave (cw) chemical lasers generally operate at pressures of the order of 1 Torr in order to achieve good efficiency. At this pressure level, the gain medium is inhomogeneously broadened. In addition, the lasing process tends to modify the gain medium so that the lasing particles are neither in translational nor rotational equilibrium. Nonetheless, early analytic models of cw chemical laser performance assumed that the lasing medium was in translational and rotational equilibrium (e.g., Refs. 1 and 2). In these models, reasonable estimates were provided for net output power, but the spectral content was not predicted. The latter requires consideration of finite translational and rotational relaxation rates.

Subsequently, analytic models and numerical codes were developed that included either rotational nonequilibrium[3-5] or translational nonequilibrium.[6-8] A recent review of rotational nonequilibrium rate processes and models is given in Ref. 9.

The combined effect of translational and rotational nonequilibrium has received less attention. An analytic model for a low pressure CO_2 laser is presented in Ref. 10, whereas a model for a generic molecular laser with applications to CO_2 and cw chemical lasers is presented in Ref. 11. A numerical code that treats both translational and rotational nonequilibrium has been developed by D. Bullock and co-workers;[12] limited numerical results have been published.[13]

The present study generalizes a previous simple model[6-8] in order to include rotational as well as translational nonequilibrium effects. The object is to provide analytic expressions for cw chemical laser amplifier and oscillator performance as well as to delineate the parameters that characterize nonequilibrium effects. The appropriate equations are first deduced. Equilibrium and nonequilibrium solutions are then obtained. Symbols are defined in Appendix A.

II. FORMULATION

Equations are deduced that define effects of translational and rotational nonequilibrium on cw chemical laser performance.

A. Flow model

A cw chemical laser is illustrated in Fig. 1a. The present simplified mixing model is illustrated in Fig. 1b. The reactants are assumed to be premixed but do not react until a flame sheet, $y_f(x)$, is reached. The flame sheet shape is specified, a priori, from diffusion theory. The streamwise station where the flame sheet reaches the channel center line is denoted x_D and characterizes the diffusion rate. The width per semichannel and the number of semichannels are denoted w and n_{sc}, respectively. Laser radiation is in the $\pm y$ direction.

B. Distribution functions

Let $n_v(J,\nu)d\nu$ denote the number of particles (moles/cm^3) with vibrational energy level v and rotational energy quantum number J that are resonant with radiation of frequency ν. The following notation is introduced

$$\int_{-\infty}^{\infty} n_v(J,\nu)d\nu \equiv n_v(J) \tag{1a}$$

$$\sum_J n_v(J) \equiv n_v \tag{1b}$$

$$\sum_v n_v \equiv n_T \tag{1c}$$

For radiation in the $\pm y$ direction, the resonant frequency ν is related to particle thermal velocity v_y by the Doppler relation

$$\frac{\nu}{\nu_o} - 1 = \pm \frac{v_y}{c} \tag{2}$$

where ν_o is the resonant frequency for particles at rest. We neglect the dependence of ν_o on v,J.

For particles with a Maxwellian thermal velocity distribution

$$\bar{p} \equiv \frac{n_v(J,\nu)}{n_v(J)} = \frac{[(4\ell n2)/\pi]^{1/2}}{\Delta\nu_d} \exp\left[-(4\ell n2)\left(\frac{\nu - \nu_o}{\Delta\nu_d}\right)^2\right] \tag{3}$$

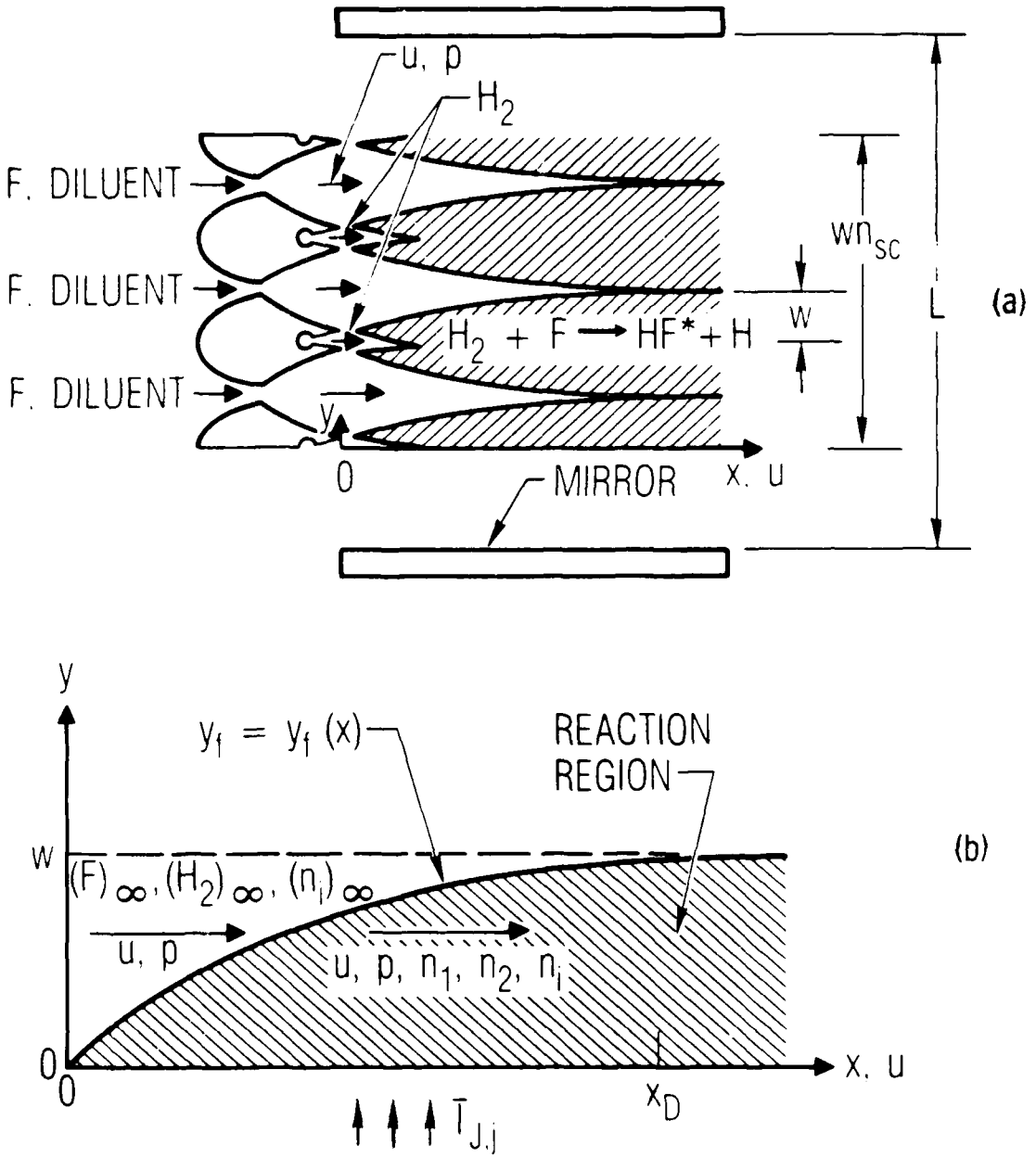

Fig. 1. Continuous Wave Chemical Laser (a) Flow Field and Fabry-Perot Resonator and (b) Flame Sheet Model of Reaction Zone[1,6-8]

where $\Delta\nu_d$ is the characteristic Doppler width (Appendix B). The value of $\bar{p}$ at line center is denoted $\bar{p}_o$ and is used to characterize the reciprocal of the Doppler width. Thus

$$\bar{p}_o = [(4\ell n2)/\pi]^{1/2}/\Delta\nu_d \tag{4}$$

We define $p_\nu = \bar{p}/\bar{p}_o$ and note

$$\int_{-\infty}^{\infty} p_\nu d\nu = \frac{1}{\bar{p}_o} \tag{5}$$

We now consider the case of rotational equilibrium and neglect the effect of vibrational energy level on the characteristic rotational energy temperature T_R. The fraction of particles in rotational energy level J is denoted $\bar{f}_J$ and is found from (Appendix B)

$$\bar{f}_J \equiv \frac{n_v(J)}{n_v} = \frac{(2J+1)\exp[-J(J+1)\vartheta_R]}{\sum_J (2J+1)\exp[-J(J+1)\vartheta_R]} \tag{6}$$

where the summation is from $J = 0$ to $J = \infty$. Let $\bar{f}_r$ denote a reference value of $\bar{f}_J$ and introduce $f_J = f_J/\bar{f}_r$. It follows that

$$\sum_J \bar{f}_J = 1 \; ; \; \sum_J f_J = 1/\bar{f}_r \tag{7}$$

Convenient values for $\bar{f}_r$ are noted in Appendix B. Finally, we observe that the gain at frequency ν for laser transition v,J can be expressed

$$g_{v,J}(\nu) = \bar{\sigma}_{v,J} \int_{-\infty}^{\infty} \left\{ \frac{2J_\ell + 1}{2J_u + 1} [n_v(J,\nu')]_u - [n_v(J,\nu')]_\ell \right\} L(\nu - \nu')d\nu' \tag{8a}$$

where subscript v,J refers to lower laser level values, subscripts u and ℓ denote upper and lower laser level values, respectively, and

$$L(\nu - \nu') = \left[1 + 4\left(\frac{\nu - \nu'}{\Delta\nu_h}\right)^2\right]^{-1} \tag{8b}$$

where $\Delta\nu_h$ is the homogeneous line width. The evaluation of $\Delta\nu_h$ and the cross section $\bar{\sigma}_{v,J}$ is discussed in Appendix B. Numerical estimates are provided in Table I.

C. Laser equations

In order to simplify the mathematical development, we assume a "Q" type laser transition

$$v + 1,\ J \rightarrow v,J \tag{9a}$$

rather than the "P" type laser transition

$$v + 1,\ J - 1 \rightarrow v,J \tag{9b}$$

appropriate for cw chemical lasers. This approximation is consistent with other simplifying assumptions used in the present model. In addition, we consider a two-vibrational energy level model and denote the upper and lower levels by subscripts 2 and 1, respectively.

The variation of upper level number density with streamwise distance, in the present model, is found from

$$\frac{u}{y_f}\frac{d[n_2(J,\nu)y_f]}{dx} = u\frac{\bar{p}\,\bar{f}_J}{y_f}\frac{d(n_T y_f)}{dx} - k_{cd}n_2(J,\nu) + k_{tr}[\bar{p}n_2(J) - n_2(J,\nu)] + k_{rr}\bar{p}[\bar{f}_J n_2 - n_2(J)] - \frac{\bar{\sigma}_{v,J}}{\varepsilon_{v,J}}[n_2(J,\nu) - n_1(J,\nu)]\sum_j L(\nu - \nu_{J,j})\bar{I}_{J,j} \tag{10a}$$

where $\varepsilon_{v,J}$ is the energy per mole of photons. The terms on the right-hand side of the equation represent the effects of chemical pumping, collisional deactivation, translational cross relaxation (assumed to be proportional to departure from translational equilibrium), rotational cross relaxation (assumed to be proportional to departure from rotational equilibrium), and stimulated emission and absorption. For the term involving k_{tr}, it is assumed that within a given rotational level J, the creation of $n_2(J,\nu)$ is proportional to the departure from translational equilibrium. For the term involving k_{rr}, it is assumed that rotational relaxation into level J results in particles with a Maxwellian velocity distribution. Equation (10a) provides the proper limits $n_2(J,\nu) \rightarrow \bar{p}n_2(J)$ and $n_2(J) \rightarrow \bar{f}_J n_2$ as $k_{tr} \rightarrow \infty$ and $k_{rr} \rightarrow \infty$,

respectively. It is assumed that the chemical reaction creates only upper level particles and that these are in translational and rotational equilibrium. The notation $\bar{I}_{J,j}$ and $\nu_{J,j}$ refers to the j^{th} resonator mode for the v + 1, J + v,J transition. The corresponding expression for the lower laser level is

$$\frac{u}{y_f}\frac{d[n_1(J,\nu)y_f]}{dx} = k_{cd}\,\bar{p}\,\bar{f}_J n_2 + k_{tr}[\bar{p}n_1(J) - n_1(J,\nu)]$$

$$+ k_{rr}\bar{p}[\bar{f}_J n_1 - n_1(J)]$$

$$+ \frac{\bar{\sigma}_{v,J}}{\epsilon_{v,J}}[n_2(J,\nu) - n_1(J,\nu)]\sum_j L(\nu - \nu_{J,j})\bar{I}_{J,j} \qquad (10b)$$

The first term on the right-hand side follows from the assumption that collisional deactivation of n_2 results in an equilibrium distribution of $n_1(J,\nu)$. The following nondimensional quantities are introduced

$$\zeta = \frac{k_{cd}x}{u} \qquad N_{2J} = \frac{n_2(J)y_f}{n_r\bar{f}_r w} \qquad (11a)$$

$$N_{2J\nu} = \frac{n_2(J,\nu)y_f}{n_r\bar{f}_r\bar{p}_o w} \qquad N_2 = \frac{n_2 y_f}{n_r w} \qquad (11b)$$

$$N^{\pm}_{J\nu} = N_{2J\nu} \pm N_{1J\nu} \qquad N^{\pm}_J = N_{2J} \pm N_{1J} \qquad (11c)$$

$$N^{\pm} = N_2 \pm N_1 \qquad I_{J,j} = \bar{I}_{J,j}/\bar{I}_{S,L} \qquad (11d)$$

$$R_t = k_{tr}/k_{cd} \qquad R_r = k_{rr}/k_{cd} \qquad (11e)$$

$$G_J(\nu') = \frac{g_J(\nu')y_f}{n_r\bar{f}_r\bar{p}_o\Delta\nu_h\bar{\sigma}_{v,J}w} \qquad G_{J,j} = G_J(\nu_j) \qquad (11f)$$

$$= \int_{-\infty}^{\infty} N^{-}_{J\nu} L(\nu - \nu')\frac{d\nu}{\Delta\nu_h} \qquad S = \pi\bar{p}_o\bar{f}_r\Delta\nu_h R_t \qquad (11g)$$

where n_r is a reference value of n_2 and

$$\bar{I}_{S,L} = \varepsilon_{\nu,J} k_{tr} / (2\bar{\sigma}_{\nu,J}) \tag{12}$$

is an intensity that characterizes line shape distortion resulting from saturation.

Substitution of normalized variables into the sum of Eqs. (10a) and (10b) and subsequent integration with respect to ν and summation with respect to J indicates

$$\frac{dN^+_{J\nu}}{d\zeta} = p_\nu f_J \frac{dN_T}{d\zeta} + p_\nu f_J N_2 - N_{2J\nu} + R_t(p_\nu N^+_J - N^+_{J\nu}) + R_r p_\nu (f_J N^+ - N^+_J) \tag{13a}$$

$$\frac{dN^+_J}{d\zeta} = f_J \frac{dN_T}{d\zeta} + (f_J N_2 - N_{2J}) + R_r(f_J N^+ - N_J^+) \tag{13b}$$

$$N^+ = N_T \tag{13c}$$

The difference between Eqs. (10a) and (10b) indicates

$$\frac{dN^-_{J\nu}}{d\zeta} = p_\nu f_J \frac{dN_T}{d\zeta} - (p_\nu f_J N_2 + N_{2J\nu}) + R_t(p_\nu N^-_J - N^-_{J\nu}) + R_r p_\nu (f_J N^- - N^-_J) - R_t N^-_{J\nu} \sum_j L(\nu - \nu_{J,j}) I_{J,j} \tag{14a}$$

$$\frac{dN^-_J}{d\zeta} = f_J \frac{dN_T}{d\zeta} - (f_J N_2 + N_{2J}) + R_r(f_J N^- - N^-_J) - \bar{p}_o \Delta\nu_h R_t \sum_j G_{J,j} I_{J,j} \tag{14b}$$

$$\frac{dN^-}{d\zeta} = \frac{dN_T}{d\zeta} - (N_T + N^-) - \frac{S}{\pi} \sum_J \sum_j G_{J,j} I_{J,j} \tag{14c}$$

Equations 13 and 14 can be solved for $N^\pm_{J\nu}$, $N^\pm_J$, and $N^\pm$, if the chemical pumping rate $dN_T/d\zeta$ is specified and if $G_{J,j}$ (oscillator) or $I_{J,j}$ (amplifier) is specified. For laminar mixing

$$N_T = (\zeta/\zeta_D)^{1/2} \tag{15}$$

where $\zeta_D = k_{cd}x_D/u$ is the normalized diffusion distance. For a Fabry-Perot resonator where each mirror has a reflectivity R_m, $g_{J,j}y_f n_{sc} = -\ell n R_m$, and

$$\frac{\bar{\sigma}_{v,J}}{\bar{\sigma}_r} G_{J,j} = \frac{-\ell n R_m}{n_{sc} n_r \bar{f}_r \bar{p}_o \Delta\nu_h \bar{\sigma}_r w} = \text{constant} \tag{16}$$

The output power per semichannel, released up to station x, is denoted $\bar{P}$ and is found from

$$P = \frac{\bar{P}}{n_r w u \varepsilon_r} = \frac{S}{2\pi} \sum_J \sum_j (\varepsilon_{v,J}/\varepsilon_r) \int_o^\zeta G_{J,j} I_{J,j} d\zeta \tag{17a}$$

If we assume $\varepsilon_{v,J} = \varepsilon_r$, Eq. (14c) indicates

$$2P = N_T - \bar{N} - \int_o^\zeta (N_T + \bar{N}) d\zeta \tag{17b}$$

The solution of these equations is discussed in the following sections.

III. EQUILIBRIUM CASES

The assumption of translational and rotational equilibrium corresponds to taking the limits $R_t \to \infty$ and $R_r \to \infty$, respectively, in Eqs. (13) and (14). The results are

$$\frac{N^+_{J\nu}}{P_\nu f_J} = \frac{N^+_J}{f_J} = N^+ = N_T \tag{18a}$$

$$\frac{N^-_{J\nu}}{P_\nu f_J} = \frac{N^-_J}{f_J} = N^- \tag{18b}$$

as expected and

$$\frac{dN^-}{d\zeta} = \frac{dN_T}{d\zeta} - (N_T + N^-) - \frac{S}{\pi} \sum_J \sum_j G_{J,j} I_{J,j} \tag{19a}$$

Also, from Eqs. (18b) and (11f), in the limit $\Delta\nu_h \ll \Delta\nu_d$,

$$\frac{2}{\pi} \frac{G_{J,j}}{f_J N^-} = \exp\left[-4\ell n2\left(\frac{\nu_j - \nu_o}{\Delta\nu_d}\right)^2\right] \left[1 + 0\left(\frac{\Delta\nu_h}{\Delta\nu_d}\right)\right] \tag{19b}$$

In the case of an oscillator, threshold gain is specified ($G_{J,j} = G_c$), and Eqs. (19a) and (19b) are solved for $I_{J,j}$. In the present two-vibrational level model, one lasing transition J,j occurs, namely the transition with highest gain. (In a multivibrational level model, there is one lasing transition for each upper vibrational level.) Amplifier solutions are obtained by specifying $I_{J,j}$ in Eq. (19a). Equations (19a) and (19b) correspond to the equilibrium model presented in Ref. 1.

IV. NONEQUILIBRIUM CASES

We now consider effects of translational and rotational nonequilibrium. The quantities R_r and R_t are large in cw chemical lasers (Table I and Ref. 9). Therefore, we consider the limit

$$R_r \gg 1, \; R_t \gg 1 \tag{20}$$

A similar approximation was introduced in Ref. 11. Simplified laser equations are deduced. Amplifier and oscillator solutions are then obtained.

A. Simplified equations

1. Limit $R_r \gg 1$, $R_t \gg 1$

Recall that number density variables in Eqs. (13) and (14) have been normalized to be of order 1. If terms of order R_r^{-1} and R_t^{-1} are neglected, Eqs. (13a)-(13c) indicate

$$\frac{N_{J\nu}^{+}}{f_J p_\nu} = \frac{N_J^{+}}{f_J} = N^{+} = N_T \tag{21}$$

Thus, $N_{J\nu}^{+}$ and N_J^{+} retain translational and rotational equilibrium distributions in the present approximation. Similarly, Eqs. (14a)-(14c) become

$$\frac{N_{J\nu}^{-}}{p_\nu f_J N^{-}} = \frac{1 + \left(\frac{R_r}{R_t} - 1\right)\left(1 - \frac{N_J^{-}}{f_J N^{-}}\right)}{1 + \sum_j L(\nu - \nu_{J,j}) I_{J,j}} \tag{22a}$$

$$\frac{N_J^{-}}{f_J N^{-}} = 1 - 2\left(\frac{\ell n 2}{\pi}\right)^{1/2} \frac{\Delta\nu_h}{\Delta\nu_d} \frac{R_t}{R_r} \sum_j \frac{G_{J,j} I_{J,j}}{f_J N^{-}} \tag{22b}$$

$$\frac{dN^{-}}{d\zeta} = \frac{dN_T}{d\zeta} - (N_T + N^{-}) - \frac{S}{\pi} \sum_J \sum_j G_{J,j} I_{J,j} \tag{22c}$$

Convection, chemical pumping, and collisional deactivation terms no longer appear in Eqs. (22a) and (22b). In the present limit, the rate of increase of $N_{J\nu}^{-}$ (or N_J^{-}) resulting from cross relaxation is just equal to the rate of loss of $N_{J\nu}^{-}$ (or N_J^{-}) resulting from stimulated emission. Thus the cross relaxation and stimulated emission processes are in equilibrium, and other rate processes

TABLE I. Numerical values of parameters for cw HF laser.
$HF:H_2:H_e:O_2 = 0.12:0.47:0.39:0.02$

(a) $v = 0$, $J = 6$, $\lambda = 2.707 \times 10^{-6}$m

$p \times 10^3$ atm	$T \times 10^{-3}$ K	$\bar{I}_{s,L}$ W/cm^2	$\bar{I}_{s,p}$ W/cm^2 B = 1.5	$\bar{I}_{s,p}$ W/cm^2 B = 7.0	$k_{cd} \times 10^{-1}$ 1/sec	$k_{tr} \times 10^{7}$ 1/sec	$R_t \times 10^{-1}$	$\Delta\omega_d \times 10^{-9}$ 1/sec	$\Delta\omega_h \times 10^{-7}$ 1/sec	$\bar{I}_1 \times 10$	$\bar{\sigma}_{v,1} \times 10^{-10}$ cm^2/mole	S
.132	.300	.085	.581E+02	.126E+04	.667	.115	1.720	.307	.036	.192	29.696	.115
.132	.600	.043	.139E+01	.295E+02	.210	.081	3.858	.434	.026	.791	41.996	.533
.132	.900	.028	.915E+00	.194E+02	.153	.066	4.327	.532	.021	1.066	51.434	.537
.132	1.200	.021	.149E+01	.320E+02	.157	.057	3.643	.614	.018	1.137	59.391	.361
1.316	.300	8.527	.655E+02	.127E+04	6.666	1.146	1.720	.307	.363	.192	2.970	1.150
1.316	.600	4.263	.317E+01	.332E+02	2.101	.811	3.858	.434	.257	.791	4.200	5.329
1.316	.900	2.842	.209E+01	.218E+02	1.529	.662	4.327	.532	.210	1.066	5.143	5.369
1.316	1.200	2.132	.265E+01	.340E+02	1.571	.573	3.643	.614	.182	1.137	5.939	3.615
13.160	.300	852.692	.253E+03	.185E+04	66.658	11.462	1.720	.307	3.634	.192	.297	11.504
13.160	.600	426.346	.247E+02	.128E+03	21.007	8.105	3.858	.434	2.569	.791	.420	53.290
13.160	.900	284.231	.163E+02	.844E+02	15.294	6.618	4.327	.532	2.098	1.066	.514	53.688
13.160	1.200	213.173	.184E+02	.100E+03	15.233	5.731	3.643	.614	1.817	1.137	.594	36.147

TABLE I. Numerical values of parameters for cw HF laser.
$HF:H_2:H_e:O_2 = 0.12:0.47:0.39:0.02$

(b) $v = 0$, $J = 9$, $\lambda = 2.823 \times 10^{-6}$m

$p \times 10^3$ atm	$T \times 10^{-3}$ K	$\bar{I}_{S,L}$ W/cm^2	$\bar{I}_{S,P}$ W/m^2 R = 1.5	R = [illegible]	[illegible] 1/sec	$k_{rr} \times$ [illegible] 1/sec	$R_f \times 10^3$	$\tau_d \times 10^{-9}$ 1/sec	$\tau_h \times$ [illegible] 1/sec	$\bar{f}_1 \times 10$	$\bar{\sigma}_{v,J} \times 10^{-10}$ cm^2/mole	S
.132	.300	[illegible]	[illegible]	[illegible]	[illegible]	.115	[illegible]	[illegible]	.036	.002	33.233	.001
.132	.600	.037	[illegible]	[illegible]	[illegible]	.081	3.858	.417	.026	.104	46.999	.073
.132	.900	.024	.819E+01	.128E+03	[illegible]	.066	[illegible]	.510	.021	.312	57.561	.164
.132	1.200	.018	.607E+01	.132E+03	[illegible]	.057	3.643	.589	.018	.497	66.466	.165
1.316	.300	2.306	.332E+06	[illegible]	6.666	1.146	[illegible]	[illegible]	.363	.002	3.323	.014
1.316	.600	3.653	.656E+02	.130E+04	[illegible]	.811	3.858	.417	.257	.104	4.700	.727
1.316	.900	2.535	.101E+02	.180E+03	1.529	[illegible]	[illegible]	.510	[illegible]	.312	5.756	1.638
1.316	1.200	1.822	.752E+01	.133E+03	1.573	.573	3.643	.589	[illegible]	.497	6.647	1.649
13.160	.300	230.619	.333E+06	.724E+02	66.658	[illegible]	[illegible]	[illegible]	[illegible]	.002	.332	.141
13.160	.600	365.310	[illegible]	.165E+04	[illegible]	[illegible]	3.858	.417	[illegible]	.104	.470	7.275
13.160	.900	243.540	.489E+02	[illegible]	[illegible]	6.618	[illegible]	.510	2.098	.312	.576	16.381
13.160	1.200	182.655	.364E+02	.235E+03	15.733	5.731	3.643	.589	[illegible]	.497	.665	16.488

TABLE I. Numerical values of parameters for cw HF laser.
$HF:H_2:H_e:O_2$ = 0.12:0.47:0.39:0.02

(c) v = 1, J = 5, $\lambda = 2.795 \times 10^{-6}$m

p × 10³ atm	T × 10⁻³ K	$\bar{I}_{S,I}$ W/cm²	$\bar{I}_{S,P}$ W/cm² B = 1.5	$\bar{I}_{S,P}$ W/cm² B = 2.0	[illegible] 1/sec	k_{rr} × [illegible] 1/sec	R_I × [illegible]	[illegible] 1/sec	[illegible] 1/sec	[illegible]	$\bar{\sigma}_{v,J} \times 10^{-10}$ cm²/mole	[illegible]
.132	.300	.039	[illegible]	[illegible]	6.068	.113	.283	.286	.036	.012	61.154	.001
.132	.600	.019	.236E+03	[illegible]	1.786	.081	.630	.404	.026	.229	86.584	.027
.132	.900	.013	.581E+02	[illegible]	.957	.066	.699	.495	.021	.510	105.921	.045
.132	1.200	.010	.591E+02	.129E+05	.983	.057	.583	.571	.018	.700	122.308	.038
1.316	.300	3.850	[illegible]	[illegible]	61.585	1.146	.283	.286	.363	.012	6.115	.013
1.316	.600	1.935	.238E+03	[illegible]	12.860	.811	.630	.404	.257	.229	8.648	.271
1.316	.900	1.283	.593E+02	[illegible]	9.573	.662	.699	.495	.210	.510	10.592	.446
1.316	1.200	.963	.600E+02	.129E+05	9.826	.573	.583	.571	.182	.700	12.231	.383
13.160	.300	385.051	.203E+06	[illegible]	605.851	11.462	.283	.286	3.634	.012	.612	.131
13.160	.600	192.531	.362E+03	[illegible]	128.596	8.105	.630	.404	2.569	.229	.865	2.710
13.160	.900	128.367	.120E+03	.138E+05	95.734	6.618	.699	.495	2.098	.510	1.059	4.460
13.160	1.200	96.260	.111E+03	.138E+05	98.264	5.731	.583	.571	1.817	.700	1.223	3.829

TABLE I. Numerical values of parameters for cw HF laser.
$HF:H_2:H_e:O_2 = 0.12:0.47:0.39:0.02$

(d) $v = 1,\ J = 8,\ \lambda = 2.911 \times 10^{-6}$m

$p \times 10^3$ atm	$T \times 10^{-3}$ K	$\bar{I}_{v,J}$ W/cm²	$\bar{I}_{v,P}$ W/cm² R = 1.5	R = 2.0	$k_{v,f} \times 10^{-?}$ 1/sec	$k_{rr} \times 10^{-7}$ 1/sec	$R_t \times 10^{-1}$	[illegible] $\times 10^{-9}$ 1/sec	$\Delta\nu_h \times 10^{-?}$ 1/sec	$\bar{\Gamma}_t \times 10$	$\bar{\sigma}_{v,J} \times 10^{-10}$ cm²/mole	S
.132	.300	.046	.135E+03	[illegible]	[illegible]	.115	.583	.298	.036	.542	53.790	.055
.132	.600	.023	.106E+02	.231E+03	1.286	.081	.630	.321	.026	1.655	76.070	.139
.132	.900	.015	.102E+02	.332E+03	.952	.066	.699	.515	.021	1.543	93.166	.113
.132	1.200	.011	.220E+02	.479E+03	.983	.057	.583	.595	.018	1.368	107.579	.068
1.316	.300	4.559	.139E+03	.293E+06	40.584	1.146	.583	.298	.363	1.212	5.379	.553
1.316	.600	2.280	.125E+02	.233E+03	17.860	.811	.630	.321	.257	1.655	7.607	1.390
1.316	.900	1.520	.120E+02	.235E+03	9.573	.662	.699	.515	.210	1.543	9.317	1.132
1.316	1.200	1.140	.230E+02	.479E+03	9.826	.523	.583	.595	.182	1.301	10.758	.684
13.160	.300	455.925	.323E+03	.332E+06	505.851	11.46[illegible]	.583	.298	[illegible]	.542	.538	5.530
13.160	.600	227.962	.558E+02	.373E+03	139.596	8.115	.630	.321	2.569	1.324	.761	13.902
13.160	.900	151.975	.460E+02	.337E+03	94.735	6.619	.699	.515	2.098	1.349	.932	11.321
13.160	1.200	113.981	.622E+02	.573E+03	98.364	5.731	.583	.595	1.817	1.301	1.076	6.836

are too slow to affect this equilibrium. The convection, chemical pumping, and collisional deactivation terms are retained in Eq. (22c), which represents global conservation. Substitution of Eq. (22a) into Eq. (11f) indicates

$$\frac{2}{\pi}\frac{G_J(\nu')}{f_J\bar{N}K_J(\nu')} = 1 + \left(\frac{R_r}{R_t} - 1\right)\left(1 - \frac{\bar{N}_J}{f_J\bar{N}}\right) \tag{23a}$$

where

$$K_J(\nu') = \frac{2}{\pi}\int_{-\infty}^{\infty} \frac{p_\nu L(\nu - \nu')}{1 + \sum_j L(\nu - \nu_{J,j})I_{J,j}} \frac{d\nu}{\Delta\nu_h} \tag{23b}$$

Equation (23) exhibits the variation of gain with frequency for a given transition v,J. The quantity $K_J(\nu')$ is the normalized line shape and is seen to depend only on $\Delta\nu_h$, $\Delta\nu_d$, and $I_{J,j}$. The coefficient of $K_J(\nu')$ in Eq. (23a) is an amplitude function and requires a knowledge of the number densities $\bar{N}$ and $\bar{N}_J$.

Evaluation of the line shape can be simplified by introduction of the variables

$$X = 2\,(\ell n2)^{1/2}(\nu - \nu_o)/\Delta\nu_d \tag{24a}$$

$$X_j = 2(\ell n2)^{1/2}(\nu_j - \nu_o)/\Delta\nu_d \tag{24b}$$

$$Y_{J,j} = (\ell n2)^{1/2}(\Delta\nu_h/\Delta\nu_d)\phi_{J,j} \tag{24c}$$

$$\phi_{J,j} = (1 + I_{J,j})^{1/2} \tag{24d}$$

For cases where $\Delta\nu_h \ll \Delta\nu_c$, the value of $K_J(\nu)$ at ν_j is affected only by the laser intensity at ν_j and is found from

$$K_J(\nu_j) \equiv K_{J,j} = \frac{(\ell n2)^{1/2}}{\pi}\frac{\Delta\nu_h}{\Delta\nu_d}\int_{-\infty}^{\infty} \frac{\exp(-X^2)dX}{Y_{J,j}^2 + (X_j - X)^2} \tag{25a}$$

$$= \frac{1}{\phi_{J,j}}\left\{\exp(-X_j^2) - \frac{2Y_{J,j}}{\pi^{1/2}}\left[1 - 2\,X_j D(X_j)\right] + O(Y_{J,j}^2)\right\} \tag{25b}$$

$$= \frac{1}{\phi_{J,j}} (\text{erfc } Y_{J,j}) \exp(Y_{J,j}^2) \; [1 + O(X_j^2)] \tag{25c}$$

where $D(X_j)$ is the Dawson integral.[14] The quantity X_j can be replaced by X in Eqs. (25a) and (25b) when $I_{J,j} = 0$. In this case, Eqs. (25a)-(25c) provide expressions for the line shape $K_J(\nu)$.

2. Limit $R_r \gg 1$, $R_t \gg 1$, $\left|R_r/R_t - 1\right| (\Delta\nu_h/\Delta\nu_d) \ll 1$

Equations (22a)-(22c) can be further simplified if it is assumed that $R_r \gg 1$, $R_t \gg 1$ and

$$\left|\frac{R_r}{R_t} - 1\right| \frac{\Delta\nu_h}{\Delta\nu_d} \ll 1 \tag{26}$$

Equations (22a), (22c), and (23a) become

$$N_{J\nu}^- = p_\nu f_J N^- / \left[1 + \sum_j L(\nu - \nu_{J,j}) I_{J,j}\right] \tag{27a}$$

$$\frac{dN^-}{d\zeta} = \frac{dN_T}{d\zeta} - N_T - (1 + B)N^- \tag{27b}$$

$$\frac{2}{\pi} G_J(\nu) = f_J N^- K_J(\nu) \tag{27c}$$

where

$$B = \frac{S}{2} \sum_J \sum_j f_J K_J(\nu_j) I_{J,j} \tag{27d}$$

These equations can be evaluated without consideration of N_J^-, which is found from

$$\frac{N_J^-}{f_J N^-} = 1 - \sqrt{\pi \ell n 2} \; \frac{\Delta\nu_h}{\Delta\nu_d} \; \frac{R_t}{R_r} \sum_j K_J(\nu_j) I_{J,j} \tag{27e}$$

Note that N_J^- is reduced below its equilibrium value by an amount which, for $K_J(\nu_j) \doteq 1$, is proportional to $I_J \Delta\nu_h/\Delta\nu_d$. Equations (27a)-(27c) are the same equations that result when rotational equilibrium is assumed.

Equations (20) and (26) are realistic for low pressure cw chemical lasers, because $R_t \sim R_r \gg 1$ and $\Delta\nu_h/\Delta\nu_d \sim 10^{-2} p(\text{Torr}) \ll 1$ in these lasers (Table I). With an increase in pressure, Eq. (26) remains valid if it is

assumed that $R_r/R_t \doteq 1$. The assumption $R_r/R_t \doteq 1$ is consistent with estimates in the range $0.5 \leq R_r/R_t \leq 10$ in Refs. 9 and 11 and with the simplified nature of the present model. The present results suggest that a first estimate for the performance of cw chemical lasers can be obtained by assuming translational nonequilibrium and rotational equilibrium [Eqs. (27a)-(27c)]. The quantity N_J^- is then found from Eq. (27e).

B. Amplifier

We consider a multiline amplifier (Fig. 1b) in the limit given by Eqs. (20) and (26) and assume that the input intensity of each transition $I_{J,j}$ is specified and is independent of ζ. The quantity B in Eq. (27) is then a constant. For laminar mixing, integration of Eq. (27b), together with Eq. (27c), yield

$$\zeta_D^{1/2} N^- = (2/\pi)\zeta_D^{1/2}\, G_J(\nu)/[f_J K_J(\nu)]$$

$$= \frac{2 + B}{(1 + B)^{3/2}} \left[D[\sqrt{(1 + B)\zeta}] - \frac{[(1 + B)\zeta]^{1/2}}{2 + B} \right] \tag{28}$$

where D( ) is again the Dawson integral. Equation (28) provides the variation of N^- with streamwise distance for various values of the parameter B. Numerical results are plotted in Fig. 2. The maximum points on these curves are denoted by subscript m and are included in Table II.

Equation (28) also provides the variation of gain with frequency, streamwise distance, and saturation. The line shape corresponding to a single laser transition at frequency $X_j = 0$ and $X_j = 0.40$ is shown in Figs. 3a and 3b, respectively. The ratio of homogeneous to inhomogeneous broadening is assumed to be $\Delta\nu_h/\Delta\nu_d = 0.024$, and the corresponding low saturation hole size, $(\ell n 2)^{1/2}\Delta\nu_h/\Delta\nu_d$, is indicated. Hole size depends on $Y_{J,j}$ [Eqs. (25a)-(25c)], and the significant increase of hole size with saturation is evident. The variation of local gain with frequency at $\zeta = 0.305$, for a single laser transition of $X_j = 0.40$, is shown in Figs. 4a and 4b for $\Delta\nu_h/\Delta\nu_d = 0.024$ and 0.048, respectively. The station $\zeta = 0.305$ corresponds to the streamwise location where the zero power gain is a maximum (Table II). Increased saturation is seen to depress the entire gain curve. This is a consequence of cross relaxation.

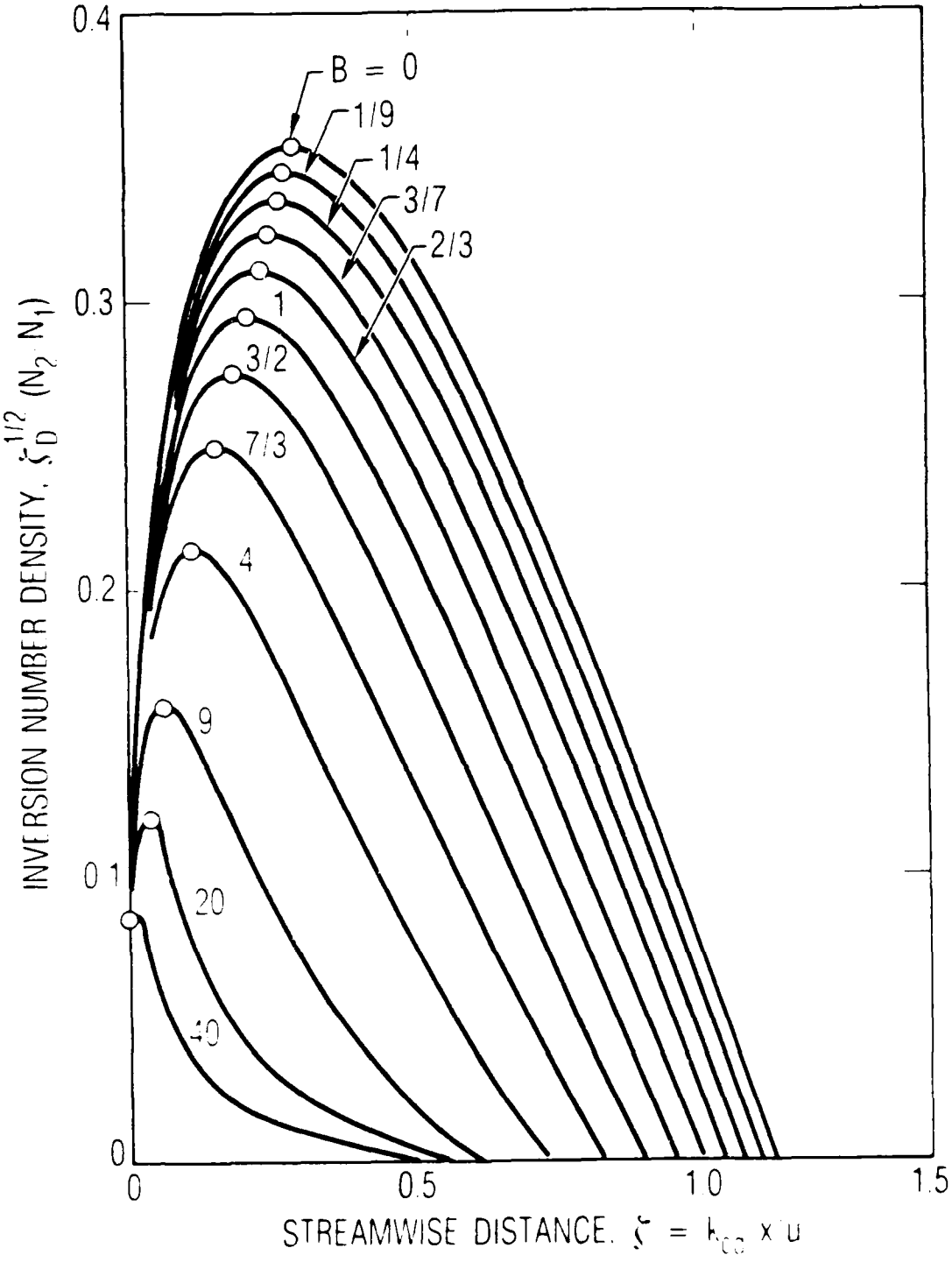

Fig. 2. Variation of Inversion Number Density with Streamwise Distance for Case of Uniformly Illuminated Amplifier with Laminar Mixing. Parameter B is a measure of saturation level.

TABLE II. Maxima for amplifier with uniform incident radiation and laminar diffusion.[a]

B	Power		Peak Inversion Number Density	
	$\frac{2\zeta_D^{1/2}P_e}{2^{1/2}/3}$	ζ_e	$\frac{\zeta_D^{1/2}N_m^-}{0.3528}$	ζ_m
0	0.0000	1.1301	1.0000	0.3051
1/9	0.0586	1.1050	0.9768	0.2926
1/4	0.1243	1.0763	0.9498	0.2788
3/7	0.1980	1.0427	0.9184	0.2629
2/3	0.2812	1.0036	0.8810	0.2438
1	0.3757	0.9566	0.8356	0.2222
1.5	0.4834	0.8992	0.7792	0.1958
7/3	0.6059	0.8273	0.7063	0.1635
4	0.7423	0.7341	0.6069	0.1237
7	0.6469	0.8491	0.5003	0.0860
9	0.8833	0.6149	0.4541	0.0714
∞	1.000	0.5000	0.000	0

[a]Eqs. (28)-(30).

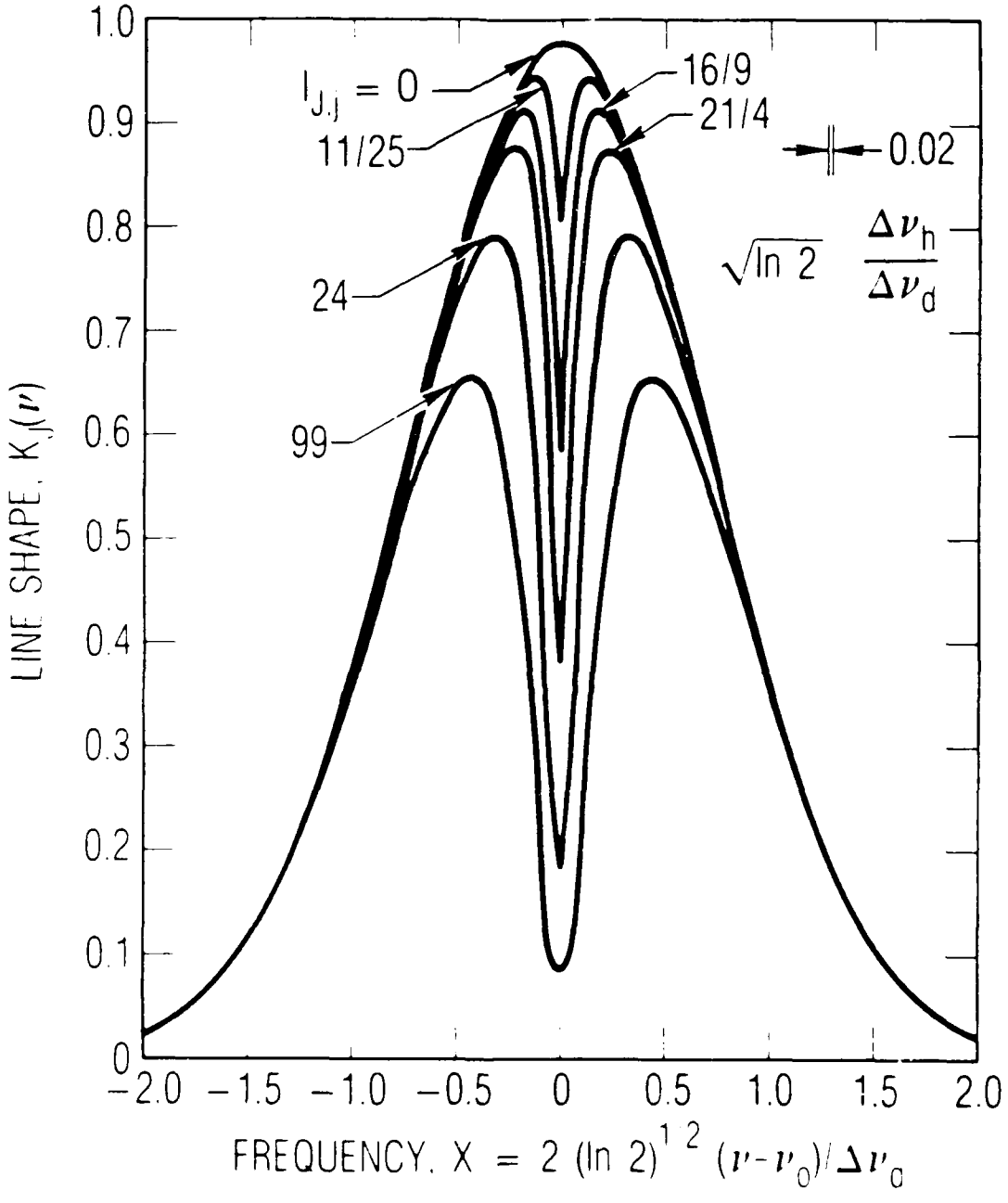

Fig. 3. Line Shape for Laser Medium with Single Transition at $X_j = 0.0$ or 0.4 and a Homogeneous Width $\Delta\nu_h/\Delta\nu_d = 0.024$ [Eq. (23b)]; (a) Case $X_j = 0.0$

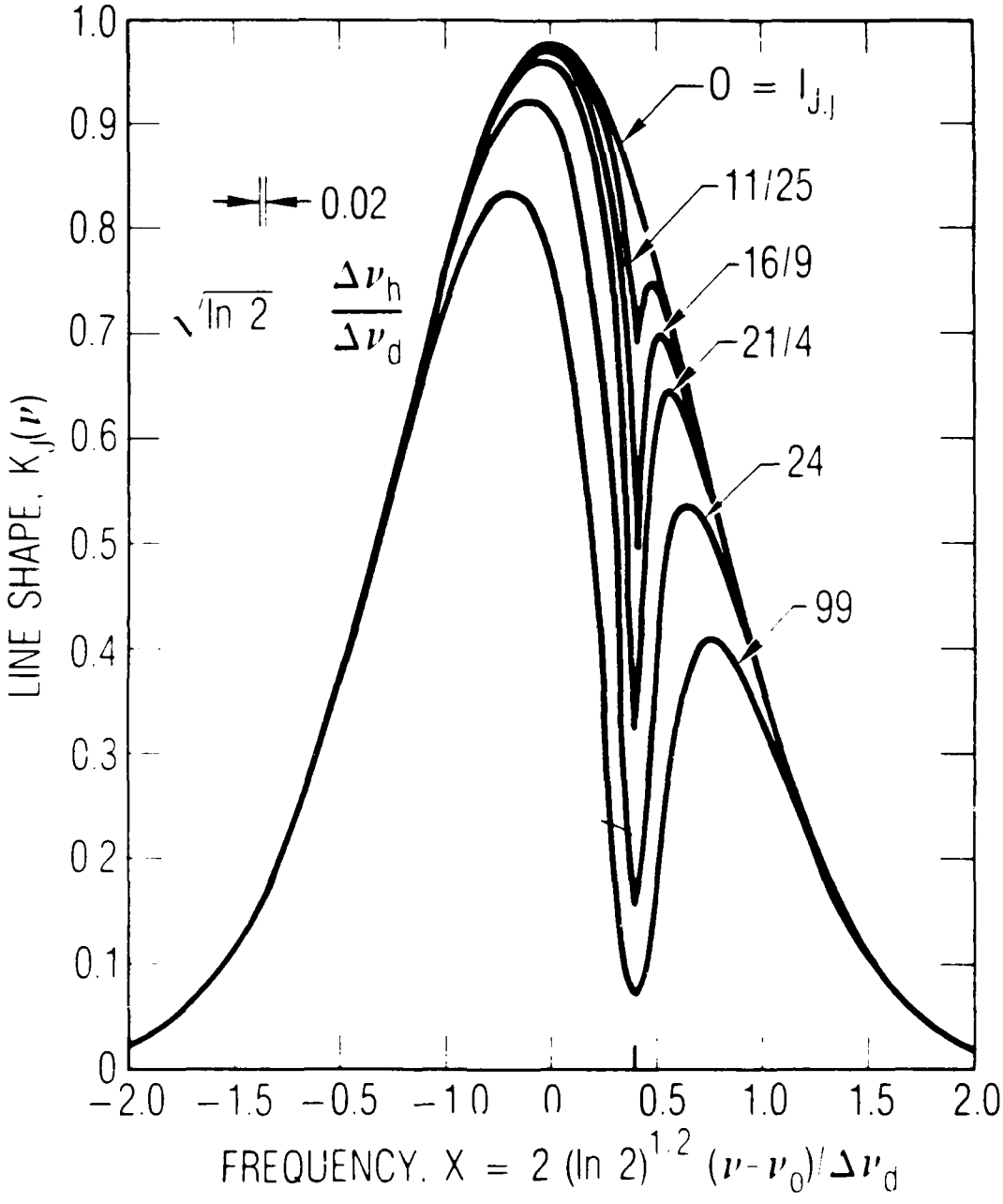

Fig. 3. Line Shape for Laser Medium with Single Transition at X_j = 0.0 or 0.4 and a Homogeneous Width $\Delta\nu_h/\Delta\nu_d$ = 0.024 [Eq. (23b)]; (b) Case X_j = 0.4

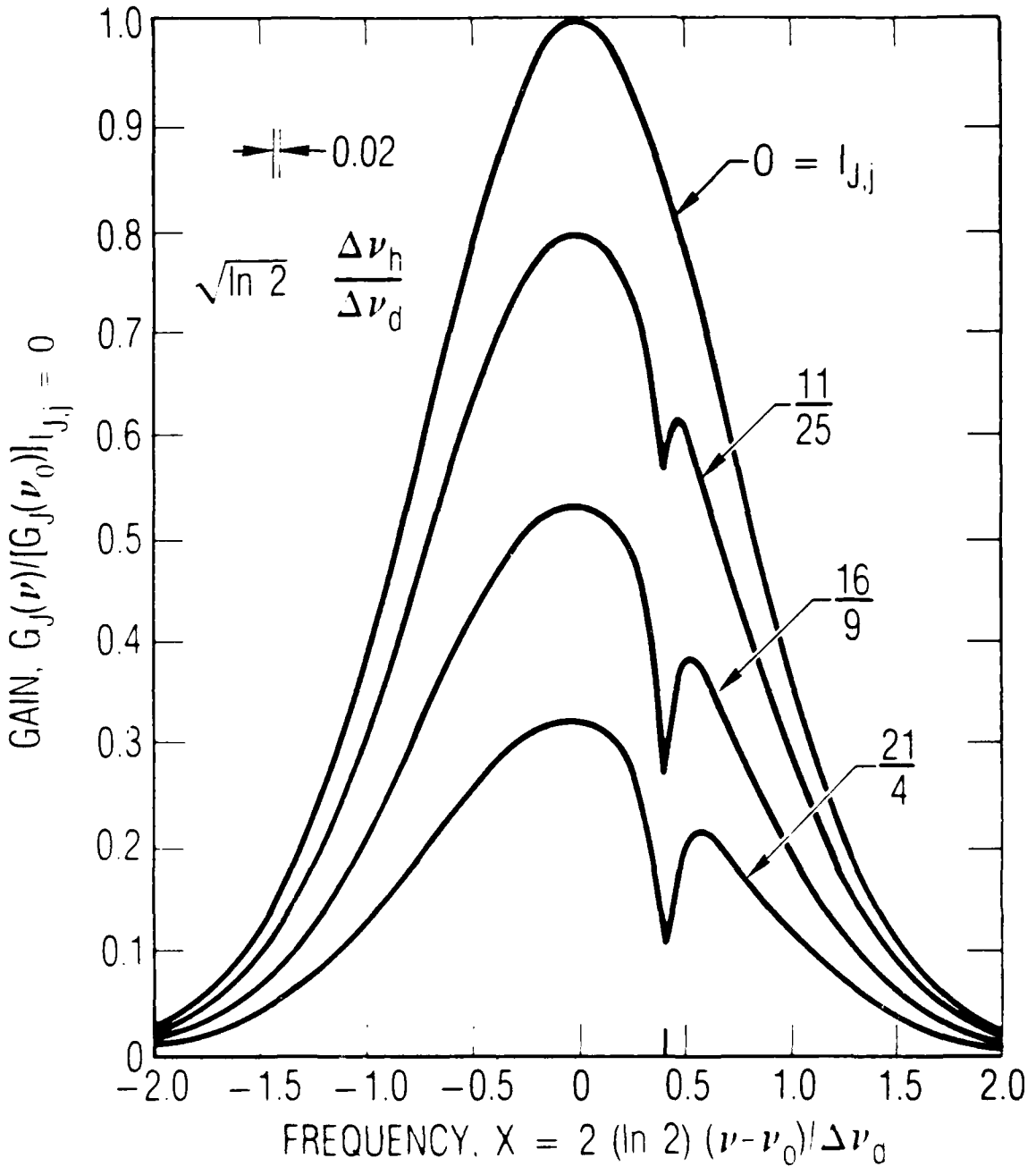

Fig. 4. Variation of Gain with Frequency at Streamwise Station $\zeta = 0.305$ in a Uniformly Illuminated Amplifier with a Single Transition at $X_j = 0.4$. Laminar mixing and homogeneous widths $\Delta\nu_h/\Delta\nu_d = 0.024$, 0.048 are assumed [Eq. (23a)]; (a) Case $\Delta\nu_h/\Delta\nu_d = 0.024$.

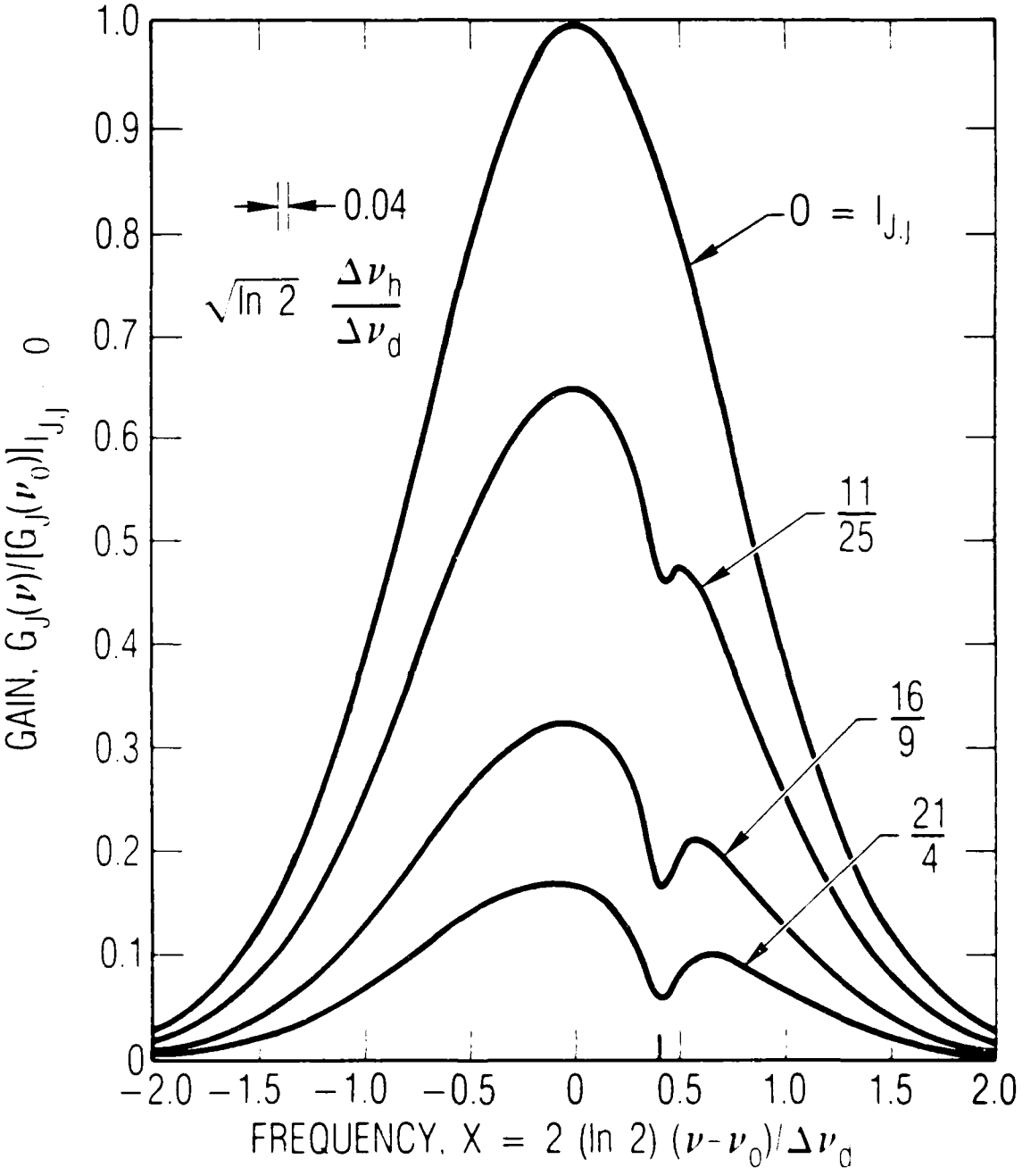

Fig. 4. Variation of Gain with Frequency at Streamwise Station $\zeta = 0.305$ in a Uniformly Illuminated Amplifier with a Single Transition at $X_j = 0.4$. Laminar mixing and homogeneous widths $\Delta\nu_h/\Delta\nu_d = 0.024, 0.048$ are assumed [Eq. (23a)]; (b) case $\Delta\nu_h/\Delta\nu_d = 0.048$.

Reference 15 reports experimental measurements of the decrease in line center gain at streamwise station $x = 0.4$ resulting from amplifier radiation at frequency $X_j = 0.40$. Figure 3a and Table Id can be used to provide theoretical estimates for line center gain variation with amplifier input intensity. The resultant estimates are included in Fig. 5 and indicate good agreement with experiment. [The authors of Ref. 15 interpreted the present line shape estimates (Fig. 3) as line center gain estimates (Fig. 4) and incorrectly concluded that the present model does not properly evaluate saturation effects.]

The downstream end of the positive gain region is denoted ζ_e and is found by equating $\bar{N}$ to zero. The result is

$$[(1 + B)\zeta_e]^{1/2} = (2 + B)D[\sqrt{(1 + B)\zeta_e}] \tag{29}$$

The net output power is

$$2\zeta_D^{1/2}P_e = [B/(1 + B)]\zeta_e^{1/2}[1 - (2/3)\zeta_e] \tag{30}$$

Corresponding values of B, ζ_e, and P_e are included in Table II. For a saturated ($B \to \infty$) amplifier

$$\zeta_e = 1/2 \; ; \; 2\zeta_D^{1/2}P_e = 2^{1/2}/3 \tag{31}$$

Equations (28)-(31) are identical in form to the corresponding results presented in Ref. 1. The parameter B in these equations replaces the parameter K_2 in Ref. 1. The previous results neglect hole burning effects on $K_{J,j}$.

The single-line amplifier solution provides a convenient basis for investigating the saturation process in cw chemical lasers. The effect of saturation on normalized line shape is determined by the parameter $I_{J,j}$. For an inhomogeneous medium, the intensity $I_{J,j} = 1$ results in a reduction of $K_{J,j}$ by a factor of $2^{-1/2}$ [Eqs. (24d) and (25b)]. The effect of saturation on power extraction is characterized by the parameter B, as indicated in Table II. In the limit $B \to \infty$, all available power is extracted by a single line. For the case of a single lasing transition, a power extraction saturation intensity $\bar{I}_{S,P}$ can be defined by Eq. (27d)

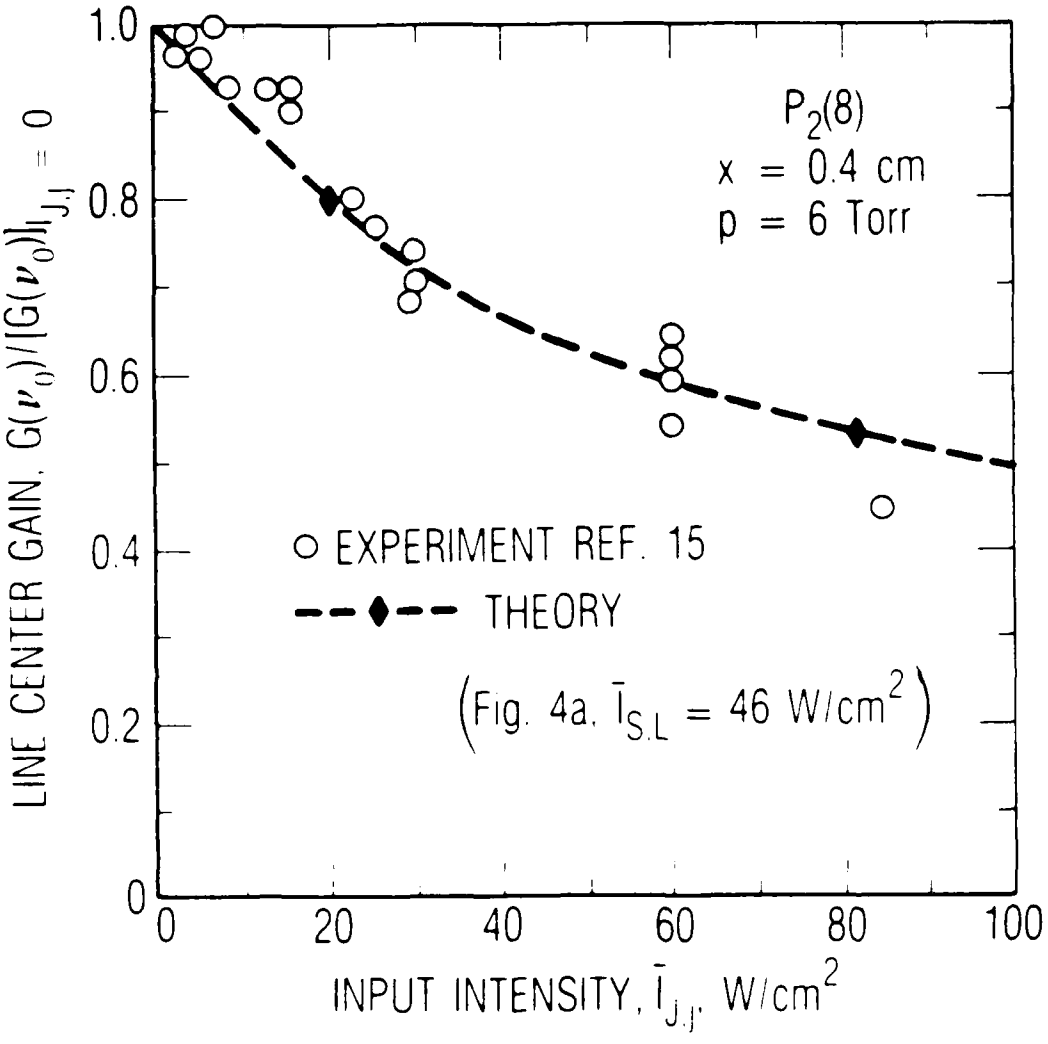

Fig. 5. Effect of Input Intensity on Line Center ($\nu = \nu_o$) Gain at Fixed Streamwise Station for Uniformly Illuminated Amplifier. Circles denote experimental data from Ref. 15 that were taken at x = 0.4 cm with a gain medium at p = 6 Torr and a laser transition corresponding to v,J = 1,8 and X_J = 0.4. The symbol ♦ denotes present estimate for gain based on line center values from Fig. 4a and $\bar{I}_{S,L}$ = 46 W/cm^2. The estimate for $I_{S,L}$ is obtained by interpolation from Table Ia by recalling $\bar{I}_{S,L} \sim p^2$ and by assuming p = 6 Torr and T = 900 K. Note also, Table Id indicates $\Delta\nu_h/\Delta\nu_d$ = 0.025, which is consistent with use of Fig. 4a.

$$\bar{I}_{S,P}/\bar{I}_{S,L} = [\beta^2 + (\beta^4 + 4\beta^2)^{1/2}]/2 \tag{32}$$

where

$$\beta = 2B/(Sf_J\phi_{J,j}K_{J,j})$$

Values of $\bar{I}_{S,P}$, corresponding to B = 1.5 and B = 7.0, are included in Table I and are seen to be large when S is small. For cases with N strong laser transitions and $\Delta\nu_h \ll \Delta\nu_c$, the power extraction saturation intensity is approximated by Eq. (32) with β replaced by β/N.

C. Oscillator

We now consider a Fabry-Perot oscillator in the limit given by Eqs. (20) and (26) and further assume that $\Delta\nu_h \ll \Delta\nu_c$ and $Y_{J,j} \ll 1$. These assumptions simplify the line shape [Eq. 25b)]. We also assume that, within each v,J lasing band, one laser frequency corresponds to ν_o; the other laser frequencies are then symmetric about ν_o, and the present summation with respect to j, rather than thermal velocity, needs no modification.[6] The intensity $I_{J,j}$ then represents the sum of the intensities in the +y and -y directions. The case $\Delta\nu_c \ll \Delta\nu_h$ is treated in Ref. 7.

The threshold gain is denoted G_c and is a constant. The gain for each lasing transition is then, assuming $\bar{\sigma}_{v,J} = \bar{\sigma}_r$

$$G_{J,j} = (\pi/2)f_J K_{J,j} N^- = G_c \tag{33}$$

Equations (25b) and (33) yield

$$I_{J,j} = \left[\frac{f_J e^{-X_j^2} N^-}{(2/\pi)G_c}\right]^2 - 1 \tag{34a}$$

where N^- is obtained from Eq. (22c), namely

$$\frac{dN^-}{d\zeta} = \frac{dN_T}{d\zeta} - N_T - N^- - \frac{SG_c}{\pi}\sum_J\sum_j\left\{\left[\frac{f_J e^{-X_j^2} N^-}{(2/\pi)G_c}\right]^2 - 1\right\} \tag{34b}$$

Equation (34a) provides the dependence of $I_{J,j}$ on f_J and X_j at each streamwise station. The number of rotational levels and longitudinal modes that reach threshold at each streamwise station is found from the requirement that $I_{J,j} > 0$ in Eq. (34a), namely

$$f_J > (2/\pi)G_c/N^- \tag{35a}$$

$$X_j^2 < \ell n[N^- f_J/(\tfrac{2}{\pi} G_c)] \tag{35b}$$

The number of lasing transitions increases as G_c/N^- decreases. Equation (34b) cannot, in general, be integrated in closed form. Two subcases are treated: a saturated multiline oscillator and a partially saturated single line oscillator.

1. Saturated multiline oscillator

Assume that $G_c << 1$ and $S = O(1)$. In this limit, $N^- << 1$ and $N^-/G_c^{1/2} = O(1)$. The laser is saturated, and there is a large number of laser transitions. Equations (34a) and (34b) become

$$(N^-)^2 = \frac{4G_c}{\pi S} \frac{dN_T/d\zeta - N_T}{\sum_J f_J^2 \sum_j e^{-2X_j^2}} \tag{36a}$$

$$I_{J,j} = \frac{\pi}{SG_c} \frac{(dN_T/d\zeta - N_T) f_J^2 e^{-2X_j^2}}{\sum_J f_J^2 \sum_j e^{-2X_j^2}} \tag{36b}$$

Corresponding number densities are

$$\frac{N_{J\nu}^-}{p_\nu f_J N^-} = \frac{1}{1 + L(\nu - \nu_{J,j})I_{J,j}} \tag{36c}$$

$$\frac{N_J^-}{f_J N^-} = 1 - \frac{dN_T/d\zeta - N_T}{\bar{f}_r R_r f_J N^-} \frac{f_J^2}{\sum_J f_J^2} \tag{36d}$$

For cases where the rotational energy levels and longitudinal mode frequencies are closely spaced, the summations in Eqs. (36a)-(36d) can be replaced by

$$\sum_j e^{-2X_j^2} = \frac{1}{2}\left(\frac{\pi}{2\ell n 2}\right)^{1/2} \frac{\Delta\nu_d}{\Delta\nu_c}\left[1 + O\left(\frac{\Delta\nu_c}{\Delta\nu_d}\right)\right]$$

$$\sum_J f_J^2 = \frac{1}{2(\bar{f}_r)^2}\left(\frac{\pi\theta_R}{2}\right)^{1/2}\left[1 + O(\theta_R)\right]$$

Equations (36) and (26b) provide the net inversion N^- and the lasing intensity $I_{J,j}$ at each streamwise station. The quantities

$$I_{J,j}/I_J = e^{-2X_j^2}/\sum_j e^{-2X_j^2} \tag{37a}$$

$$I_J/I = f_J^2/\sum_J f_J^2 \tag{37b}$$

are plotted in Figs. 6a and 6b for $G_c \to 0$. Longitudinal mode intensity $I_{J,J}$ is inversely proportional to $\Delta\nu_d/\Delta\nu_c$, which is a measure of the number of longitudinal modes with a significant amount of power. The dependence of I_J on θ_R is indicated in Fig. 6b. The number of active lasing modes decreases as G_c increases. Equation (36c) indicates that $N_{J\nu}^-$ departs from the equilibrium value $p_\nu f_J N^-$ only in the vicinity of each lasing frequency $\nu_{J,j}$. The departure from equilibrium is large because $I_{J,j}$ is large. The departure of N_J^- from the equilibrium value $f_J N^-$ is of order $1/(R_r N^-)$.

Because the laser is saturated, the output power and mode length are $2\zeta_D^{1/2}P_e = 2^{1/2}/3$ and $\zeta_e = 1/2$, respectively, for laminar mixing. Thus, for the saturated multiline oscillator, rotational and translational nonequilibrium impact spectral output but not output power.

2. Single line oscillator

The parameters S and G_c determine the degree of saturation. In order to investigate their influence, we consider a case where line selection results in a single laser transition. For convenience, consider laminar mixing, $f_J = 1$, and $X_J = 0$. Lasing is initiated at station ζ_i, where the gain first reaches the threshold value. Integration of Eq. (34b) with $I_{J,j} = 0$ indicates

$$\zeta_D^{1/2} N_i^- = (2/\pi)\zeta_D^{1/2} G_c = 2D(\zeta_i^{1/2}) - \zeta_i^{1/2} \tag{38}$$

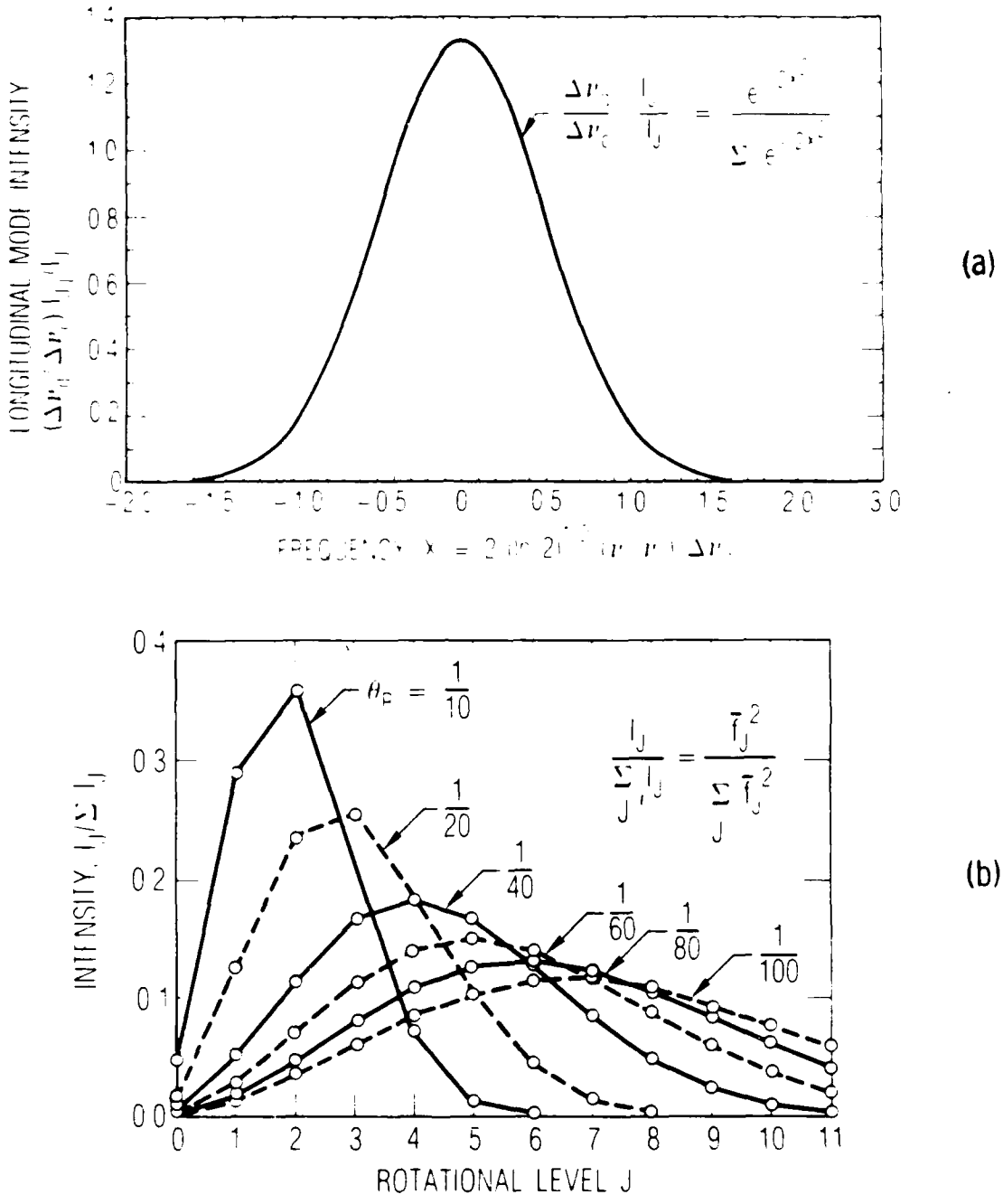

Fig. 6. Performance of Saturated Multiline Fabry-Perot Oscillator in the Limit $R_r = R_t \gg 1$, $\Delta\nu_h \ll \Delta\lambda_c$, $Y_{J,j} \ll 1$, $G_c \to 0$, and $S = 0(1)$ [Eqs. (36) and (37)]. (a) Variation of longitudinal mode intensity $I_{J,j}$ with frequency X_j and (b) variation of intensity I_J with rotational level J.

which agrees with Eq. (28) for B = 0. Equation (38) provides ζ_i and $\zeta_D^{1/2}N_i^-$ for a given value of $\zeta_D^{1/2}G_c$. Downstream of ζ_i

$$\frac{d\zeta_D^{1/2}N^-}{d\zeta} = \frac{1}{2\zeta^{1/2}} - \zeta^{1/2} - \zeta_D^{1/2}N^- - \frac{S}{2}\zeta_D^{1/2}N_i^-\left[\left(\frac{N^-}{N_i^-}\right)^2 - 1\right] \tag{39}$$

which is integrated with the initial condition $N^- = N_i^-$ at $\zeta = \zeta_i$. Lasing terminates at the downstream station ζ_e, where $N^- = N_i^-$. The net output power is

$$2\zeta_D^{1/2}P_e = \left[\zeta^{1/2} - (2/3)\zeta^{3/2}\right]_{\zeta_i}^{\zeta_e} - \int_{\zeta_i}^{\zeta_e}\zeta_D^{1/2}N^-d\zeta \tag{40}$$

Equations (39) and (40) have been evaluated for several values of S and $\zeta_D^{1/2}G_c$. Output power is given in Fig. 7 and decreases as S and G_c are reduced.

Oscillator solutions where hole burning effects are neglected correspond to $S \to \infty$, $I_{J,j} \to 0$, and $SI_{J,j}$ = finite. The number density in the lasing region is a constant given by $N^- = N_i^-$, where N_i^- and ζ_i are obtained from Eq. (38). The local lasing intensity for laminar mixing is

$$2\zeta_D^{1/2}\frac{dP}{d\zeta} = \frac{1}{2\zeta^{1/2}} - \zeta^{1/2} - \zeta_D^{1/2}N_i^- \tag{41}$$

The end of the lasing region occurs when the intensity goes to zero, or

$$\zeta_e = \left\{\left[\left(\zeta_D^{1/2}N_i^-\right)^2 + 2\right]^{1/2} - \zeta_D^{1/2}N_i^-\right\}^2/4 \tag{42}$$

The net output power is found from Eq. (40) and is included in Fig. 7. Neglect of hole burning is seen to overestimate output power.

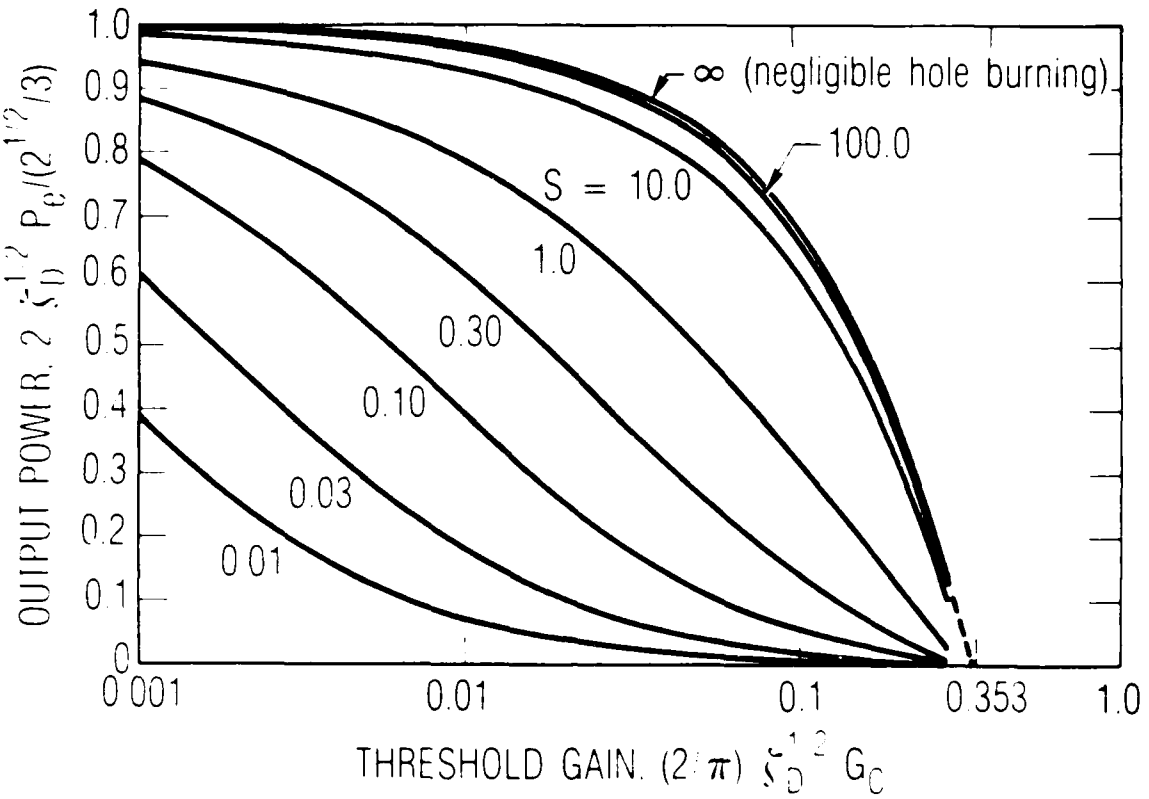

Fig. 7. Performance of Single Line Fabry-Perot Oscillator in Limit $R_r = R_t \gg 1$ and $Y_{j,j} \ll 1$.

V. DISCUSSION

The parameters that characterize laser performance are discussed further, and numerical estimates are provided.

The parameters introduced in the present study may be expressed in the form

$$R_t \sim \frac{k_{tr}}{k_{cd}} \frac{n_2(J,\nu)}{n_2(J,\nu)} \sim \frac{\text{Particle Collision Rate}}{\text{Particle Deactivation Rate}} \tag{43a}$$

$$I_{J,j} \sim \frac{(\bar{\sigma}_{v,J}/\varepsilon_{v,J})\bar{I}_{J,j}}{k_{tr}} \frac{n_2(J,\nu)}{n_2(J,\nu)} \sim \frac{\text{Particle Stim. Emission Rate}}{\text{Particle Collision Rate}} \tag{43b}$$

$$S \sim \frac{k_{tr}}{k_{cd}} \frac{\Delta\nu_h n_2(J,\nu)}{n_2} \sim \frac{\text{Resonant Particle Collision Rate}}{\text{Net Deactivation Rate}} \tag{43c}$$

$$B \sim \frac{\sum_J \sum_j \frac{\bar{\sigma}_{v,J}}{\varepsilon_{v,J}} \bar{I}_{J,j}}{k_{cd}} \frac{\Delta\nu_n n_2(J,\nu)}{n_2} \sim \frac{\text{Net Stim. Emission Rate}}{\text{Net Deactivation Rate}} \tag{43d}$$

$$G_c S \sum_J \sum_j I_{J,j} \sim \frac{\sum_J \sum_j \frac{\bar{I}_{J,j}}{\varepsilon_{J,j}} \frac{g_c y_f}{w}}{k_{cd} n_2} \sim \frac{\text{Net Stim. Emission Rate}}{\text{Net Deactivation Rate}} \tag{43e}$$

The parameter R_t may be viewed as the number of translational collisions an upper level particle undergoes before it is collisionally deactivated. The parameter $I_{J,j}$ represents the ratio of particle stimulated emission rate to particle collisional deactivation rate. Similarly, S represents the ratio of the collisional deactivation rate of particles resonant with $I_{J,j}$ to the net upper level particle collisional deactivation rate. Finally, B and $G_c S \sum_J \sum_j I_{J,j}$ apply to amplifiers and oscillators, respectively, and represent the ratio of net stimulated emission rate to net collisional deactivation rate. The latter ratio characterizes laser output power and efficiency.

Numerical estimates for parameters and rate coefficients are included in Table I for a fixed stoichiometry, $300 < T, K < 1200$, $0.132 < p, atm < 13.2$ ($0.10 < p, Torr < 10.0$), and v,J = 0, 6; 0, 9; 1,5, and 1, 8. The pressure dependence of quantities in Table I is given by

$$\frac{S}{p} \sim \frac{k_{cd}}{p} \sim \frac{k_{tr}}{p} \sim \frac{\Delta\nu_h}{p} \sim \frac{\bar{I}_{S,L}}{p^2} \sim 1 \tag{44}$$

and permits interpolation of data in Table I with regard to pressure. Values of the power saturation intensity $\bar{I}_{S,P}$ are given for B = 1.5 and 7.0. These values of $\bar{I}_{S,P}$ correspond, roughly, to achieving one-half saturated power output and one-half zero power inversion number density, respectively. Note that $\bar{I}_{S,P}$ is relatively insensitive to pressure, in contrast to $\bar{I}_{S,L}$.

VI. CONCLUDING REMARKS

In the present model we have assumed that convection, chemical pumping, and collisional deactivation rates are small compared with translational relaxation, rotational relaxation, and stimulated emission rates. Similar approximations are introduced in Ref. 11. It is expected that corresponding simplifications can be introduced into numerical codes in order to facilitate solutions.

The further assumption $\left|R_r/R_t - 1\right|(\Delta\nu_h/\Delta\nu_d) \ll 1$ resulted in a system of equations for cw chemical laser performance that are independent of N_J^-. This result suggests that a reasonable first estimate for cw chemical laser performance (other than evaluation of N_J^-) can be obtained by assuming rotational equilibrium and translational nonequilibrium, as was done in Refs. 6-8. The physical basis for the latter approximation is as follows. CW chemical lasers operate at pressures of the order of 1 Torr and are inhomogeneously broadened. The modification of line shape (i.e., hole burning), induced by lasing, is more important than lasing induced departures from rotational equilibrium.

The present results may be contrasted with those for a pulsed chemical laser. A pulsed chemical laser generally operates at pressures of the order of one atmosphere, in order to achieve high energy density and is homogeneously broadened. As a consequence, its performance is insensitive to translational nonequilibrium, and spectral output is determined from considerations of rotational nonequilibrium.

APPENDIX A. PARTIAL LIST OF SYMBOLS

B	parameter defining amplifier saturation, Eq. (27)
c	speed of light in vacuum
$D(\ )$	Dawson integral, Ref. 14
$\bar{f}_J$, f_J	fraction of particles in rotational energy level, Eq. (6)
$G_J(\nu)$, $G_{J,\nu}$	normalized gain, Eq. (11)
$g_{v,J}(\nu)$	gain, Eq. (8)
$\bar{I}_{J,j}$	intensity for longitudinal mode J,j
$\bar{I}_J$, $\bar{I}$	net intensities
$\bar{I}_{S,L}$, $\bar{I}_{S,P}$	line shape and power saturation intensities, Eqs. (12) and (32)
$I_{J,j}$	nondimensional intensity, Eq. (11d)
J	rotational energy level
j	longitudinal mode number
$K_J(\nu)$, $K_{J,j}$	line shape, Eqs. (23) and (25)
k_{cd}, k_{tr}, k_{rr}	deactivation, translational and rotational relaxation rates
$L(\nu - \nu')$	Lorentzian distribution, Eq. (8)
$N_{J\nu}$, N_J, N, N_T	normalized particle number densities, Eq. (11)
$n_v(J,\nu)$, $n_v(J)$, n_v	particle number densities, Eq. (1)
n_T	total number of lasing species, $n_1 + n_2$
P	normalized output power, Eq. (17)
$\bar{p}$, $\bar{p}_o$, p_ν	velocity distribution functions, Eqs. (3)-(5)
p	pressure
R_t, R_r	collisional rate ratios, Eq. (11e)
S	collisional deactivation rate parameter, Eq. (11h)
T	temperature
u	streamwise velocity
v_y	thermal velocity in y direction
X, X_j	normalized frequency, Eq. (24)
x	streamwise distance, Fig. 1
x_D	characteristic diffusion distance, Fig. 1
$Y_{J,j}$	homogeneous width parameter, Eq. (24)
y	transverse distance, Fig. 1
$\varepsilon_{v,J}$	energy per mole of photons
ζ	normalized streamwise distance $k_{cd}x/u$

ζ_D	normalized diffusion distance, $k_{cd}x_D/u$
θ_R	characteristic rotational temperature parameter, Eq. (6)
λ	wavelength
ν	frequency
ν_o	line center frequency
$\Delta\nu_d$	Doppler width [full-width, half-maximum (FWHM)]
$\Delta\nu_h$	homogeneous width (FWHM)
$\Delta\nu_c$	longitudinal mode separation, c/2L
$\bar{\sigma}_{v,J}$	cross section for stimulated emisssion, Eq. (B-8)
$\phi_{J,j}$	$(1 + I_{J,j})^{1/2}$

Subscripts

e	end of lasing region
i	start of lasing region
J	rotational level
j	longitudinal mode
m	maximum value
r	reference value or rotational relaxation value
v	vibrational level

Superscripts

+	sum of number densities, Eq. (11)
-	difference of number densities, Eq. (11)

APPENDIX B. PARAMETER EVALUATION

Expressions needed to evaluate parameters of interest are noted below.

B.1 Dopper width [full-width, half-maximum (FWHM)]

$$\Delta\nu_d = 2\left(\frac{2kT\ell n2}{Mc^2}\right)^{1/2}\nu_o \qquad \text{sec}^{-1}$$

$$= (831.6/\lambda)(T/300)^{1/2}(20/M)^{1/2} \tag{B-1}$$

where λ is wavelength in meters and M is molecular weight.

B.2 Homogeneous width (FWHM)

$$\pi T^{1/2}\frac{\Delta\nu_h}{p} = \sum_i \frac{p_i}{p}\bar{\gamma}_i \qquad \frac{(K)^{1/2}}{\text{atm-sec}} \tag{B-2}$$

where $\bar{\gamma}_i$ is $2\pi cT^{1/2}\gamma_i$ and γ_i is tabulated in Ref. 7. Values of $\bar{\gamma}_i$ are given in Table III.

B.3 Gas kinetic collision rate ($HF + M_i \rightarrow HF + M_i$)

$$T^{1/2}\frac{k_{gk}}{p} = \sum_i \frac{p_i}{p} a_i \qquad \frac{(K)^{1/2}}{\text{atm-sec}} \tag{B-3}$$

where

$$a_i = T^{1/2}\frac{(k_{gk})_i}{p_i} = \frac{N_A^{3/2}}{R_o}\left[8\pi k\left(\frac{1}{M_{HF}} + \frac{1}{M_i}\right)\right]^{1/2}\left[\frac{d_{HF} + d_i}{2}\right]^2$$

Values of a_i are included in Table III. For a billiard ball model, $\bar{\gamma}_i = a_i$ and $\pi\Delta\nu_h = k_{gk}$.

TABLE III. Homogeneous width and gas kinetic collision rate data for $HF + M_i \rightarrow HF + M_i$.[a]

M_i	Gas kinetic rate $a_i \times 10^{-11}$ $(K)^{1/2}$/atm-sec	Homogeneous widths Rotational Level J	$\bar{\gamma}_i \times 10^{-11}$ $(K)^{1/2}$/atm-sec
HF	0.77	6 → 10	9.1 → 3.3
DF		6 → 10	5.7 → 3.0
H_2	1.95	5 → 9	1.1 → 0.73
N_2	1.00	6 → 8	1.2 → 0.87
H_e	1.28	All	0.16
A_r	0.86	6 → 8	0.16 → 0.49
O_2	0.92		
F_2	0.86		

[a]Refs. 2 and 6.

B.4 Vibrational deactivation rate

We consider vibrational deactivation of the form

$$HF(v + 1) + M_i \xrightarrow{\bar{k}^i_{cd}} HF(v) + M_i \qquad \text{(B-4)}$$

The net deactivation rate k_{cd} is then

$$\frac{k_{cd}}{p} \equiv -\frac{1}{p}\frac{d\ell n\ HF(v+1)}{dt} = \sum_i \frac{p_i}{p}\frac{\bar{k}^i_{cd}}{R_o T} \qquad \frac{1}{\text{atm-sec}} \qquad \text{(B-5)}$$

Values of $\bar{k}^i_{cd}/(R_o T)$ are given in Table IV.

B.5 Rotational equilibrium

For rotational equilibrium, the fraction of particles with rotational energy $J(J + 1)kT_R$ is given by

$$\frac{n_v(J)}{n_v} \equiv \bar{f}_J = \frac{(2J+1)\exp[-J(J+1)\theta_R]}{\sum_J (2J+1)\exp[-J(J+1)\theta_R]} \qquad \text{(B-6a)}$$

$$= \theta_R(2J+1)\exp[-J(J+1)\theta_R][1 + O(\theta_R)] \qquad \text{(B-6b)}$$

where the summation is from $J = 0$ to $J = \infty$, $\theta_R = T_R/T$, and $T_R \doteq 30.16$ K for HF. The maximum value of $\bar{f}_J$ and the corresponding value of J, associated with a fixed value of θ_R, are denoted $\bar{f}_{J,m}$ and J_m, respectively. Typical values are included in Table V. For a fixed value of θ_R, the quantity $\bar{f}_{J,m}$ provides a convenient value for the reference quantity $\bar{f}_r$. When $\bar{f}_r = \bar{f}_{J,m}$

$$f_J \equiv \frac{\bar{f}_J}{\bar{f}_r} = \frac{(2J+1)\exp[-J(J+1)\theta_R]}{(2J_m+1)\exp[-J_m(J_m+1)\theta_R]} \qquad \text{(B-6c)}$$

and $f_J < 1$ for $J \neq J_m$.

B.6 Photon energy

Photon energy, per mole, is

TABLE IV. Vibrational deactivation rates for reaction

$$HF(v+1) + M_i \xrightarrow{\bar{k}^{1}_{cd}} HF(v) + M_i^{a}$$

M_i	$\bar{k}^{1}_{cd}$ $(cm^3/(mole\text{-}sec))$	$\frac{1}{(v+1)^n}\frac{\bar{k}^{1}_{cd}}{R_0 T}$ $(atm\text{-}sec)^{-1}$			
		300 K	600 K	900 K	1200 K
HF	$(v+1)^{2.6}\,(3\times10^{14}\,T^{-1}+1.5\times10^{5}\,T^{2.76})$	4.2×10^{7}	1.15×10^{7}	6.76×10^{6}	5.78×10^{6}
F	$(v+1)^{2.7}\,(1.9\times10^{13}\,e^{-1359/T})$	8.32×10^{6}	4.01×10^{7}	5.68×10^{7}	6.22×10^{7}
H_2	$(v+1)^{2.7}\,(6\times10^{11}\,T^{-1}+10^{5}\,T^{2.28})$	2.62×10^{5}	4.59×10^{5}	7.56×10^{5}	1.07×10^{6}
A_r, F_2	$(v+1)^{2.7}\,(2\times10^{5}\,T^{2.5})$	1.14×10^{7}	1.29×10^{8}	5.33×10^{8}	1.46×10^{9}
H_2O	$(v+1)^{2.7}\,(3.7\times10^{-5}\,T^{3.5})$	2.11×10^{7}	2.39×10^{8}	9.86×10^{8}	2.70×10^{9}

[a] Based on Ref. 14, where $R_0 = 82.06\ (cm^3\text{-}atm)/(mole\text{-}K)$

TABLE V. Maximum value of $\bar{f}_J$ and corresponding value of J for fixed θ_R.

θ_R	J_m	$\bar{f}_{J,m}$
1/10	2	0.2654
1/20	3	0.1889
1/40	4	0.1353
1/60	5	0.1106
1/80	6	0.0957
1/100	7	0.0854

$$\varepsilon_{v,J} = N_A h\nu = 0.1196/\lambda \quad \text{J/mole} \tag{B-7}$$

where λ is in meters.

B.7 Gain coefficient

The gain coefficient for a P-branch transition $v + 1, J - 1 \rightarrow v, J$ can be expressed[2]

$$\frac{\pi}{2} \Delta\nu_h \frac{\bar{\sigma}_{v,J}}{\varepsilon_{v,J}} = \frac{B(v,J,-1)}{4\pi} \qquad \frac{cm^2}{J\text{-sec}} \tag{B-8}$$

where $B(v,J,-1)$ is the Einstein coefficient.[2] For HF, the latter can be approximated by

$$B(v,J,-1) = 3.79 \times 10^{13} \frac{2J(1+v)}{2J+1} (1 + 0.063J) \left(1 - \frac{0.01v^3}{1+v}\right)$$

which is believed to be correct to within about 10% for $1 \leq J \leq 16$ and $v \leq 6$.

REFERENCES

1. H. Mirels, R. Hofland, and W. S. King, "Simplified Model of CW Diffusion Type Chemical Laser," AIAA J. 11 (12), 156-164 (February 1973).
2. G. Emanuel, "Numerical Modeling of Chemical Lasers," Handbook of Chemical Lasers," edited by R. W. F. Gross and J. F. Bott (John Wiley and Sons, 1976), pp. 488-496.
3. R. J. Hall, "Rotational Nonequilibrium and Line-Selected Operation in cw DF Chemical Lasers," IEEE J. of Quantum Electron. QE-12, 453-462 (August 1976).
4. L. H. Sentman and W. Rushmore, "Computationally Efficient, Rotational Nonequilibrium cw Chemical Laser Model," AIAA J. 19 (10), 1323 (October 1981).
5. T. T. Yang, "Modeling of cw HF Chemical Laser with Rotational Nonequilibrium," J. de Phys. Colloque C9 41 (11), C9-51 (November 1980).
6. H. Mirels, "Inhomogeneous Broadening Effects in cw Chemical Lasers," AIAA J. 17 (5), 478-489 (May 1979).
7. H. Mirels, "Inhomogeneous Broadening Effects in Multimode cw Chemical Lasers," Appl. Opt. 20 (2), 362-373 (15 January 1981).
8. H. Mirels, "Multimode Low Pressure cw Chemical Laser Performance Including Source Flow Effects," Appl. Opt. 20 (14), 2379-2388 (15 July 1981).
9. N. Cohen, J. F. Bott, M. A. Kwok, and R. L. Wilkins, The Status of Rotational Nonequilibrium in HF Chemical Lasers, Report No. TR-0086(6603)-2 (The Aerospace Corporation, El Segundo, CA, May 1986).
10. T. Kan and G. J. Wolga, "Influence of Collisions on Radiative Saturation and Lamb Dip Formation in CO_2 Molecular Lasers," IEEE J. of Quantum Electron. QE-7 (4), 141-150 (April 1971).
11. A. A. Stepanov and V. A. Shcheglov, "Dynamic Saturation of Optical Transitions in High Power Molecular Lasers," Soviet J. Quantum Electron. 12 (5), 619-624 (May 1982).
12. D. L. Bullock, M. M. Valley, and R. S. Lipkis, Advanced Chemical Laser Optics Study, Final Report, Contract No. F29601-79-C-0011 (TRW, 15 July 1982).
13. D. L. Bullock, J. de Phys. C9 37 (1980).
14. M. Abramowitz and I. A. Stegun, Handbook of Matnematical Functions, AMS 55 (National Bureau of Standards, June 1964), pp. 297-303.

15. R. W. F. Gross and J. C. Coffer, "Saturation Processes in Doppler-Broadened HF Vibrational Transition," in Gas Flow and Chemical Lasers, edited by M. Onorato (Plenum Press, 1984), pp. 127-139.

16. N. Cohen and J. F. Bott, Review of Rate Data For Reactions of Interest in HF and DF Lasers, Report No. TR-0083(3603)-02 (The Aerospace Corporation, El Segundo, CA, October 1982).

LABORATORY OPERATIONS

The Aerospace Corporation functions as an "architect-engineer" for national security projects, specializing in advanced military space systems. Providing research support, the corporation's Laboratory Operations conducts experimental and theoretical investigations that focus on the application of scientific and technical advances to such systems. Vital to the success of these investigations is the technical staff's wide-ranging expertise and its ability to stay current with new developments. This expertise is enhanced by a research program aimed at dealing with the many problems associated with rapidly evolving space systems. Contributing their capabilities to the research effort are these individual laboratories:

Aerophysics Laboratory: Launch vehicle and reentry fluid mechanics, heat transfer and flight dynamics; chemical and electric propulsion, propellant chemistry, chemical dynamics, environmental chemistry, trace detection; spacecraft structural mechanics, contamination, thermal and structural control; high temperature thermomechanics, gas kinetics and radiation; cw and pulsed chemical and excimer laser development including chemical kinetics, spectroscopy, optical resonators, beam control, atmospheric propagation, laser effects and countermeasures.

Chemistry and Physics Laboratory: Atmospheric chemical reactions, atmospheric optics, light scattering, state-specific chemical reactions and radiative signatures of missile plumes, sensor out-of-field-of-view rejection, applied laser spectroscopy, laser chemistry, laser optoelectronics, solar cell physics, battery electrochemistry, space vacuum and radiation effects on materials, lubrication and surface phenomena, thermionic emission, photosensitive materials and detectors, atomic frequency standards, and environmental chemistry.

Computer Science Laboratory: Program verification, program translation, performance-sensitive system design, distributed architectures for spaceborne computers, fault-tolerant computer systems, artificial intelligence, microelectronics applications, communication protocols, and computer security.

Electronics Research Laboratory: Microelectronics, solid-state device physics, compound semiconductors, radiation hardening; electro-optics, quantum electronics, solid-state lasers, optical propagation and communications; microwave semiconductor devices, microwave/millimeter wave measurements, diagnostics and radiometry, microwave/millimeter wave thermionic devices; atomic time and frequency standards; antennas, rf systems, electromagnetic propagation phenomena, space communication systems.

Materials Sciences Laboratory: Development of new materials: metals, alloys, ceramics, polymers and their composites, and new forms of carbon; nondestructive evaluation, component failure analysis and reliability; fracture mechanics and stress corrosion; analysis and evaluation of materials at cryogenic and elevated temperatures as well as in space and enemy-induced environments.

Space Sciences Laboratory: Magnetospheric, auroral and cosmic ray physics, wave-particle interactions, magnetospheric plasma waves; atmospheric and ionospheric physics, density and composition of the upper atmosphere, remote sensing using atmospheric radiation; solar physics, infrared astronomy, infrared signature analysis; effects of solar activity, magnetic storms and nuclear explosions on the earth's atmosphere, ionosphere and magnetosphere; effects of electromagnetic and particulate radiations on space systems; space instrumentation.

...

END

DATE

FILMED

5-88

DTIC